Supplemental Materials

Mosaic loss of Chromosome Y in aged human microglia.

Michael C. Vermeulen[1], Richard Pearse[2], Tracy Young-Pearse[2], Sara Mostafavi[3]

[1] Center for Molecular Medicine and Therapeutics, University of British Columbia, Vancouver, Canada
[2] Department of Neurology, Harvard Medical School, Boston, USA
[3] Paul G. Allen School of Computer Science and Engineering, University of Washington, Seattle, USA

Corresponding Author
Sara Mostafavi, Ph.D.
saramos@cs.washington.edu
185 E Stevens Way NE
Seattle, WA 9819

Table of Contents

Supplemental Methods

Single-cell RNAseq dataset curation

ROSMAP study datasets

Single-cell microglia data from 'Olah' and 'Mathys' originated from fresh autopsy and frozen tissues from two longitudinal aging studies: Rush Religious Order Study (ROS) and Rush Memory and Ageing Project (MAP). Raw FASTQ files were obtained via Synapse from https://www.synapse.org/#!Synapse:syn12514624 ('Olah') and https://www.synapse.org/#!Synapse:syn18485175 ('Mathys'). A summary of all information collected on the ROSMAP cohort is available at www.radc.rush.edu.

Single-cell pre-processing

Including intronic UMIs to improve LOY estimation sensitivity

Accompanying the biological findings in this study, technical improvements regarding LOY detection using scRNA-seq were made. Mainly, we found that including introns for UMI counting significantly increased detected genes with minimal impact on clustering. In 10x Chromium 3' single-cell assays, to uniquely barcode each individual RNA molecule, poly(dT) primers are designed to prime poly(A) mRNA tails. Poly(dT) primers can also prime internal, often intronic, poly(A) tracts resulting in intronic UMIs from mature RNA (Technical note: 10x Genomics CG000376 - Rev A; https://assets.ctfassets.net/an68im79xiti/awNZTarmwqmwxKcvDv9wv/b05500661e36290b8ce59689ff889ea8/CG000376_TechNote_Antisense_Intronic_Reads_SingleCellGeneExpression_RevA.pdf). Because intronic UMIs are commonly derived from a biological molecule and are correlated with exonic UMI counts, they represent a valuable information source that improves transcriptional sensitivity for calling LOY with scRNA-seq.

Initial scRNA-seq dataset preprocessing and annotation

All single-cell and single-nuclei processing was performed using Seurat (v4.0.2). A basic template is provided in **Supplemental Code**. Filtered expression matrices were normalized using the *NormalizeData* function using the log normalize method and a scale factor of 10000. The top 2500 variable genes were determined using *FindVariableFeatures* using the *vst* method. Gene expression matrices were scaled and centered using *ScaleData* where the effects of nUMI, percent mitochondrial UMI and percent ribosomal UMI variables were regressed out. Principal components analysis (PCA) was performed using *RunPCA* and UMAP using *RunUMAP*. All ribosomal genes, mitochondrial genes, male–specific genes, female–specific genes (XIST) were removed from the variable features list prior to PCA calculation. PC selection for UMAP and clustering was determined using the elbow method. Clustering was performed using *FindNeighbors* (default settings) and *FindClusters* using 0.1 resolution. Datasets were visually inspected for sample and batch–specific clustering patterns. If biases were observed, batch correction was applied using Harmony (v1.0.0) (Korsunsky et al. 2019). Cell type annotations were determined through an iterative approach of increasing resolution using both automatic annotation through SingleR (Aran et al. 2019) and traditional annotation using differentially expressed canonical marker genes (**Supplemental Fig. S21**; **Supplemental Code**). Differentially expressed genes in each cluster were determined using MAST (Finak et al. 2015) via *FindAllMarkers*. Latent variables in each MAST model included nUMI, nGenes, ribosomal UMI pct expressed, donor, and brain region (when multiple tissues were present in an individual study).

Microglia subcluster processing and annotation

For microglia subcluster analysis, marker gene lists were derived from previous publications (**Supplemental Table S8**). Each member of a specific subtype classification (i.e., H1, H2) is not consistently distinct between datasets. Leiden clusters defined using *FindClusters* were each labelled with a microglia subtype based on gene set enrichment using *AddModuleScore*. Homeostatic microglia (H) were primarily determined using *C3, CD74, CX3CR1* and *P2RY12*.

Neuron-associated homeostatic microglia subtypes additionally expressed *CTNNA2*, *NAV3*^{hi} and *GRID2*. Disease associated microglia (DAM) marker genes included *APOE, LPL, CD63, CD83, MYO1E, SPP1* and *DSCAM*. Inflammatory subtypes (I) were commonly enriched for age-associated microglia modules and were determined using *CD163, TGFB1,* and *DPYD*. Cytokine response microglia (CRM) were primarily determined using *CCL3, CCL4* and *IL1B*. Cycling microglia were annotated using *MKI67*, *CENPP, BRIP1, TOP2A* and the KEGG cell-cycle gene set. Interferon response microglia (IRM) were annotated using *IFI27, IFI44L, IFIT1, IFIT2* and *IFIT3*. As a result of high environmental sensitivity, single-cell isolation can induce a stressed phenotype in microglia (Thrupp et al. 2020). Stressed microglia were labelled using dissociation-associated microglia genes from Thrupp *et al.* including *FOS, JUN, JUNB* and *DUSP*. CNS-associated macrophages, which include perivascular and meningeal macrophages, were annotated using *CD163*^{hi}, *F13A1* and *LYVE1*. Monocytes were annotated using *VCAN*, *CCR2*, and *FCN1*. Blood-derived tumor-associated macrophages were annotated using *KYNU, VAV3*, and *TGFBI* in addition to a tumor associated macrophage marker gene set (Müller et al. 2017). For **Fig. 4**, and **Supplemental Fig. S15**, microglia, and astrocytes from the GSE160936 dataset (Smith et al. 2022) were isolated by brain region of origin (SSC or EC) and processed as above. Through the Seurat workflow, canonical correlation analysis (CCA) was used to integrate microglia populations. We followed the scRNA-seq integration vignette provided by the Satija Lab (https://satijalab.org/seurat/articles/integration_introduction.html) and used default settings. Density contouring for LOY and non-LOY nuclei/cells was done using the *dittoDimPlot* function from the dittoSeq package (Bunis et al. 2020). Contours were added using the 'do.contour' flag. Kernel gene-weighted density estimation was performed using the Nebulosa package (Alquicira-Hernandez et al. 2021).

Determining technical confounders of donor-level LOY

We found that the sequencing depth and feature diversity in a single-cell transcriptome were strongly correlated with LOY estimates (**Supplemental Fig S7B**). Limiting the dataset to high-information cells/nuclei dampens this effect. Setting sequencing thresholds at >=3000 UMI and >=1000 genes significantly reduces association between LOY estimates and UMI depth. This suggests that with sufficient sequencing depth single-cell GEX LOY estimates become increasingly stable and less prone to stochastic MSY gene dropout. To determine additional technical confounders to LOY across donors, we regressed a set of potential confounders against LOY proportion. Linear regression was performed for each cell type using the *lm* function including pairwise tests between LOY percentage and each of the following variables: total cell/nuclei number, MSY gene sparsity score, normalized Chr Y expression, 10x chemistry/version, mean UMI depth, and donor age.

Male–specific Y Chromosome expression sparsity filtering and adjustment

Within a cell type population/cluster, single-cell LOY estimates are strongly associated with the sparsity of male–specific Y (MSY) gene expression within Chromosome Y expressing cells (**Supplemental Fig. S7**). To remove the technical confounder of insufficient MSY expression we filtered and adjusted our data using a metric we call MSY sparsity score. To calculate this score, within each cell type cluster we first subset for cells with evidence of Y Chromosome presence (MSY UMI >= 1) and iteratively calculated the percentage of cells expressing each detected MSY gene using Seurat *DotPlot*. To generate the raw sparsity value, percent expressed values of each MSY gene were summed. Sparsity values were determined for each cell type cluster/population in each donor and were later subjected to scaling and centering. When making LOY frequency estimates cell type populations with MSY sparsity score < -1.75 were removed (**Supplemental Fig. S4B**).

We further used MSY sparsity scores to adjust LOY estimates. Using LOY percentage estimates and MSY sparsity scores from a collection of 1.4 million male cells (**Supplemental Data S1**) we calculated the non-linear least squares best fit using a 2-parameter exponential decay model (DRC.expoDecay) (**Supplemental Fig. S7; Supplemental Code**). After fitting the brain LOY data to this model, positive residuals were taken as adjusted LOY percentage estimates, and negative residuals were set to 0. Simply, our adjusted LOY estimate represents the deviation above expected LOY given the sparsity of the Chr Y-proficient cells in their cluster/population.

Removed samples and datasets

Datasets from accessions syn16780177, syn22130805, PRJNA434002 were considered but were removed because of low sequencing depth and feature diversity. Subject MD5893 from GSE126836 was considered low quality and was removed.

Sex chromosome disorder bulk RNAseq analysis (GSE126712)

The GSE126712 (Zhang et al. 2020) dataset contains PBMC transcriptomes from Turner syndrome (45,XO; *n*=13), Klienfelter's syndrome (47,XXY; *n*=14) and control (46,XX, *n*=15; 46,XY, *n*=13) (**Supplemental Fig S22**). Bulk RNAseq expression matrices were downloaded from GEO accession GSE126712 and processed using edgeR. Normalization factors were determined using TMM and expression values were converted to CPM and log normalized. Genes with low read counts were removed using *filterByExpr* with default settings. Differential expression analysis was performed using limma/voom. The design matrix was constructed using sex chromosome ploidy (i.e., XO = 1; XX/XY = 2; XXY = 3). Multiple statistical testing was controlled using FDR < 0.01 (Benjamini-Hochberg). DE genes were considered if the absolute value logFC > 0.3. Plots were generated using the ggplot2, ggpubr and pheatmap packages.

Single nuclei multiome ATAC and gene expression analysis

The multimodal LOY analysis was performed on sample data provided by 10x Genomics (https://www.10xgenomics.com/resources/datasets/fresh-frozen-lymph-node-with-b-cell-lymphoma-14-k-sorted-nuclei-1-standard-2-0-0). The dataset contains joint scATAC-seq and scRNA-seq for ~14,000 nuclei from an intra-abdominal lymph node tumor from a male patient diagnosed with non-Hodgkin lymphoma. Filtered feature barcode matrices (HDF5) and fragment files were downloaded from 10x Genomics and processed using both Seurat (v4.0.2) (Hao et al. 2021) and Signac (v1.2.1) (Stuart et al. 2021), following the Signac 10x scATAC vignette (https://satijalab.org/signac/articles/pbmc_vignette.html). Briefly, ATAC data was normalized using TF-IDF and features in the 75th quartile were considered top features. Peaks were identified using Cellranger and peaks within blacklist regions were removed (blacklist_hg38_unified). Gene expression pre-processing was performed as above, and dimension reduction and clustering were performed solely using the transcriptome. HG38 gene annotations from standard chromosomes were added from EnsDb.Hsapiens.v86.

Supplemental Results

Investigation of LOY in AD and control snRNA-seq from EC and SSC (Smith et al.)
Corresponds with Figure 4.

Consistent with our initial LOY analysis, across all Smith et al. samples and brain regions LOY nuclei were most common in the microglia (1917 / 10222; 15.79%; range (donor) = 1.84%–56.98%) and rare in neuronal (4 / 1136; 0.15%; range = 0%-0.86%) and astrocyte (182 / 30,659; 0.59%; range = 0.19%-2.41%) populations (**Fig. 6**). 48,748 QC'd nuclei were retained including 32,122 astrocyte (65.9%), 13,222 microglia (27.1%), and 1,304 neuronal nuclei (2.67%) from 4 AD and 4 control donors. All samples displayed high per cell UMI counts (median = 6,386; IQR = 6,788.7), gene counts (median = 2,758; IQR = 1824.7), sufficient nuclei sample size (mean nuclei per sample = 3,585.1; SD = 1,439.2), and robust Y Chromosome expression in biological replicates, therefore providing a quality opportunity to compare LOY in glial cells between AD and control samples (**Fig. 6**; **Supplementary Fig. S15**). Endothelial cells (48 / 410; 10.48%), OPCs (27 / 323; 7.77%), pericytes (42 / 571; 6.85%) and oligodendrocytes (9 / 157; 5.73%) also showed elevated LOY rates, however sample sizes were considerably smaller and prone to variation. LOY microglia were observed in every subject but were primarily seen in microglia populations of 4 samples from 2 AD donors: A096 (Age: 87; SSC LOY: 40.3%; EC LOY: 47.5%) and A163 (Age: 83; SSC LOY: 46.2%; EC LOY: 61.8%; Supplemental Fig. S26). These 2 subjects harbored 70.3% of the LOY population in the Smith et al. dataset.

We and others (Dumanski et al. 2021; Mattisson et al. 2021) have found cells/nuclei with fewer UMI counts and greater expression sparsity have an increased probability of false-positive LOY calls through random dropout of all Y Chromosome genes. To confirm that LOY estimates were not a result of low sequencing depth we called LOY using increasing minimum UMI thresholds (**Supplemental Results Fig. S1A**). In both the EC and SSC samples, as the minimum UMI threshold was increased from 1000 to 6000, microglia LOY frequency remained stable, while in astrocyte and neuronal populations LOY frequencies approached 0. Furthermore, in astrocyte and neuronal populations, LOY nuclei have significantly lower mean UMI and feature counts than non-LOY/normal nuclei (**Supplemental Results Fig. S1B,C**), while in microglia these attributes are not significantly different between the groups. Together, this suggests in the Smith et al. dataset that we are observing biologically meaningful LOY nuclei in the microglia, whereas in astrocyte and neuronal populations LOY labelled cells/nuclei are more likely to be a result of technical and stochastic factors.

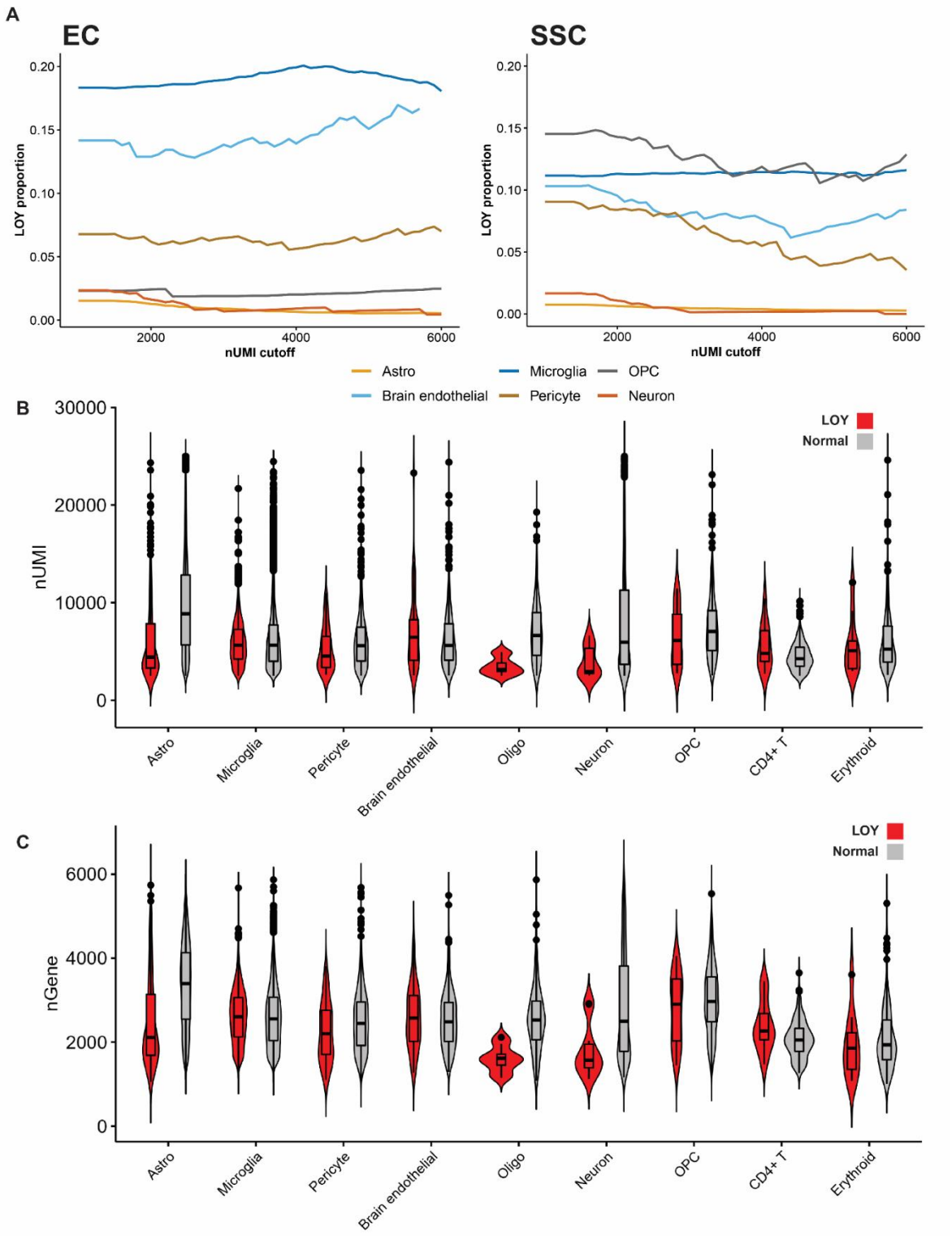

Supplemental Results Figure S1: Attributes compared between LOY and non-LOY nuclei within each cell type cluster (GSE160936). (*A*) LOY frequencies in each cell type as nUMI thresholds are increased for (*Left*) entorhinal cortex (EC) and (*Right*) somatosensory cortex (SSC) derived nuclei. Each colored line represents an individual cell type cluster. LOY frequencies are quite stable as UMI thresholds increase suggesting LOY classification is not overly confounded by sequencing depth. In both brain regions, with more UMI information astrocytes and neurons approach LOY frequencies of 0 while microglia maintain frequencies > 10%. *B-C*, Violins and boxes show (*B*) UMI counts and (*C*) detected genes (nGenes) in LOY (red) and non-LOY (grey) nuclei for each cell type cluster. Data from both EC and SSC samples are included.

Supplemental Figures

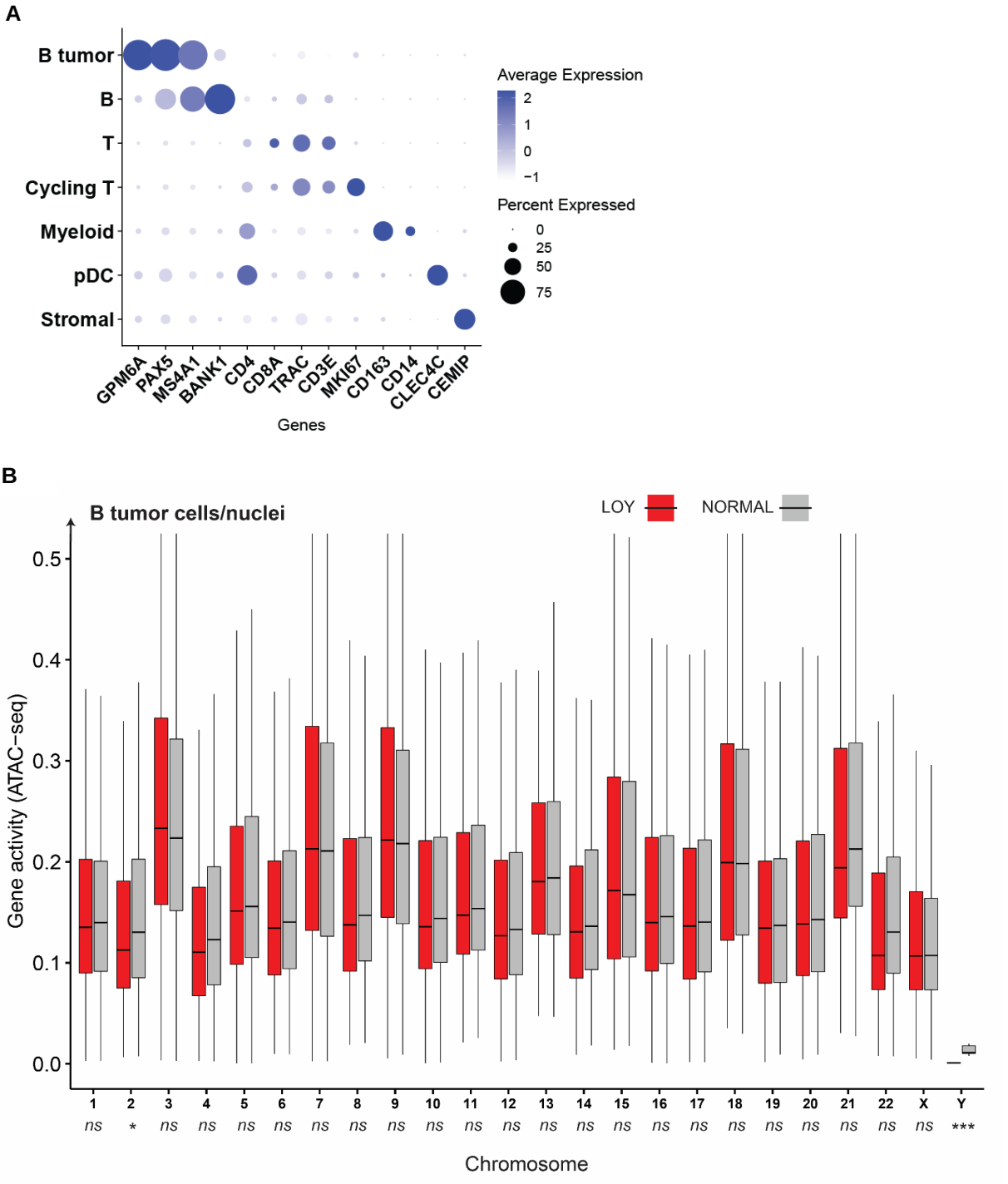

Supplemental Figure S1: (*A*) Marker genes used to annotate Leiden-based clusters with cell types. *GPM6A* and *PAX5* were used to differentiate cancerous and non-cancerous B cells. (*B*) Comparison of LOY and non-LOY/normal chromatin accessibility-based gene activity across all chromosomes in B tumor nuclei (n = 1,895). LOY was classified using the gene expression (GEX) assay. B tumor nuclei were included if they contained >1500 GEX UMI, >1000 GEX features, >10000 ATAC UMI and > 1000 ATAC genes. Gene activity scores were calculated using genes with > 0.2 mean normalized expression and > 0 gene activity across all nuclei from the chromosome of interest. Tests of difference between LOY and normal groups for each chromosome are provided along the *x*-axis. Wilcoxon test: (*ns*) $P > 0.01$, (*) $P < 0.01$, (***) $P < 0.0001$.

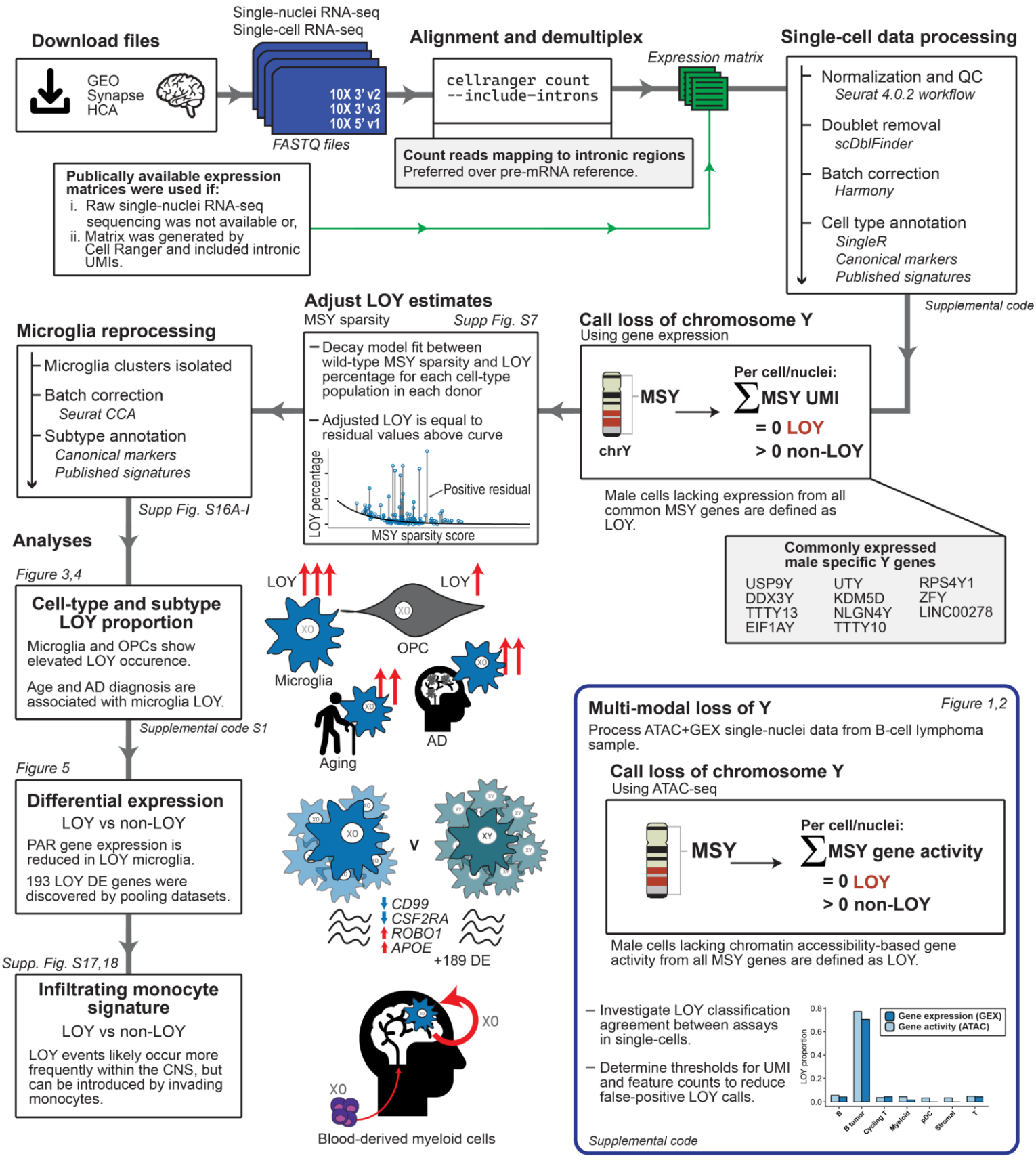
Download files
GEO
Synapse
HCA
Single-nuclei RNA-seq
Single-cell RNA-seq
10X 3' v2
10X 3' v3
10X 5' v1
FASTQ files
Alignment and demultiplex
cellranger count
--include-introns
Count reads mapping to intronic regions
Preferred over pre-mRNA reference.
Expression matrix
Single-cell data processing
Normalization and QC
Seurat 4.0.2 workflow
Doublet removal
scDblFinder
Batch correction
Harmony
Cell type annotation
SingleR
Canonical markers
Published signatures
Supplemental code
Publically available expression matrices were used if:
i. Raw single-nuclei RNA-seq sequencing was not available or,
ii. Matrix was generated by Cell Ranger and included intronic UMIs.
Adjust LOY estimates
MSY sparsity
Supp Fig. S7
Decay model fit between wild-type MSY sparsity and LOY percentage for each cell-type population in each donor
Adjusted LOY is equal to residual values above curve
LOY percentage
Positive residual
MSY sparsity score
Call loss of chromosome Y
Using gene expression
MSY
chrY
Per cell/nuclei:
∑MSY UMI
= 0 LOY
> 0 non-LOY
Male cells lacking expression from all common MSY genes are defined as LOY.
Commonly expressed male specific Y genes
USP9Y
DDX3Y
TTTY13
EIF1AY
UTY
KDM5D
NLGN4Y
TTTY10
RPS4Y1
ZFY
LINC00278
Microglia reprocessing
Microglia clusters isolated
Batch correction
Seurat CCA
Subtype annotation
Canonical markers
Published signatures
Supp Fig. S16A-I
Analyses
Figure 3,4
Cell-type and subtype LOY proportion
Microglia and OPCs show elevated LOY occurence.
Age and AD diagnosis are associated with microglia LOY.
Supplemental code S1
Figure 5
Differential expression
LOY vs non-LOY
PAR gene expression is reduced in LOY microglia.
193 LOY DE genes were discovered by pooling datasets.
Supp. Fig. S17,18
Infiltrating monocyte signature
LOY vs non-LOY
LOY events likely occur more frequently within the CNS, but can be introduced by invading monocytes.
LOY
LOY
OPC
Microglia
AD
Aging
V
CD99
CSF2RA
ROBO1
APOE
+189 DE
X0
X0
Blood-derived myeloid cells
Multi-modal loss of Y
Figure 1,2
Process ATAC+GEX single-nuclei data from B-cell lymphoma sample.
Call loss of chromosome Y
Using ATAC-seq
MSY
Per cell/nuclei:
∑MSY gene activity
= 0 LOY
> 0 non-LOY
Male cells lacking chromatin accessibility-based gene activity from all MSY genes are defined as LOY.
Investigate LOY classification agreement between assays in single-cells.
Determine thresholds for UMI and feature counts to reduce false-positive LOY calls.
Gene expression (GEX)
Gene activity (ATAC)
LOY proportion
B
B tumor
Cycling T
Myeloid
pDC
Stromal
T
Supplemental code

Supplemental Figure S2: Bioinformatic workflow for single-cell and single-nuclei pre-processing and LOY analysis. Flow diagram illustrates the study design and bioinformatic steps used to analyze LOY in the brain. A graphical abstract of key findings, and associated figures is also provided. All single-cell and single-nuclei RNAseq data collected for this study was generated using 10x Genomics Chromium library preparation. Single-cell (sc) and single-nuclei (sn) RNAseq data was subject to slightly different alignment workflows. For scRNA-seq, to improve transcriptional sensitivity, introns were retained for UMI counting. This required all single-cell data sets to be aligned through our local pipeline using Cellranger (v5.0.0) and the "--include introns" flag. An internal 10x technical note (Interpreting Intronic and Antisense Reads in Single Cell Gene Expression Data - Rev A) (10x Genomics 2021) found that including introns for single-cell data improves nUMI and nGene counts with minimal impact on clustering. Since snRNA-seq data is commonly processed with introns included, we did not align all snRNA-seq datasets locally. Once expression matrices were generated, all subsequence pre-processing was identical between snRNA-seq and scRNA-seq datasets (Seurat).

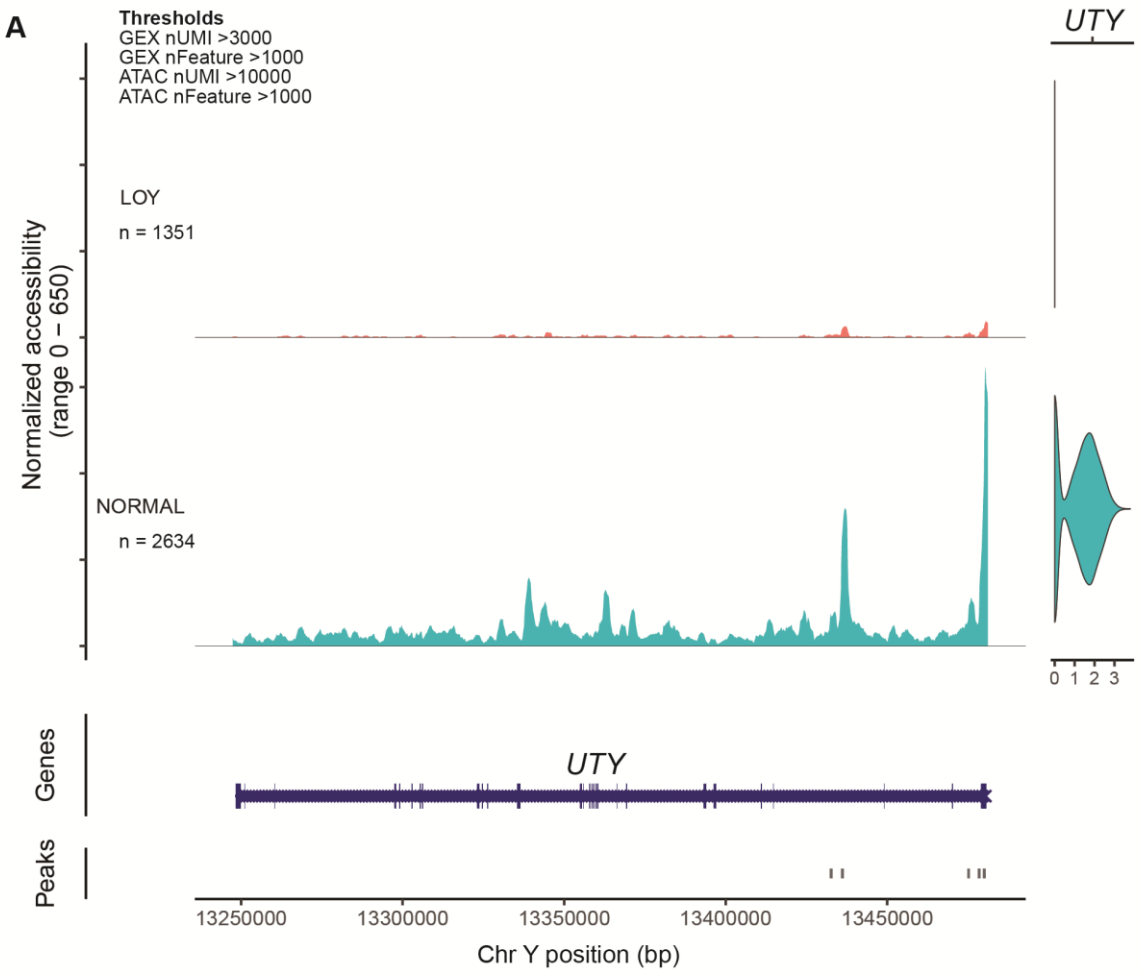
A
Thresholds
GEX nUMI >3000
GEX nFeature >1000
ATAC nUMI >10000
ATAC nFeature >1000
UTY
LOY
n = 1351
NORMAL
n = 2634
Normalized accessibility
(range 0 – 650)
0 1 2 3
Genes
UTY
Peaks
13250000
13300000
13350000
13400000
13450000
Chr Y position (bp)

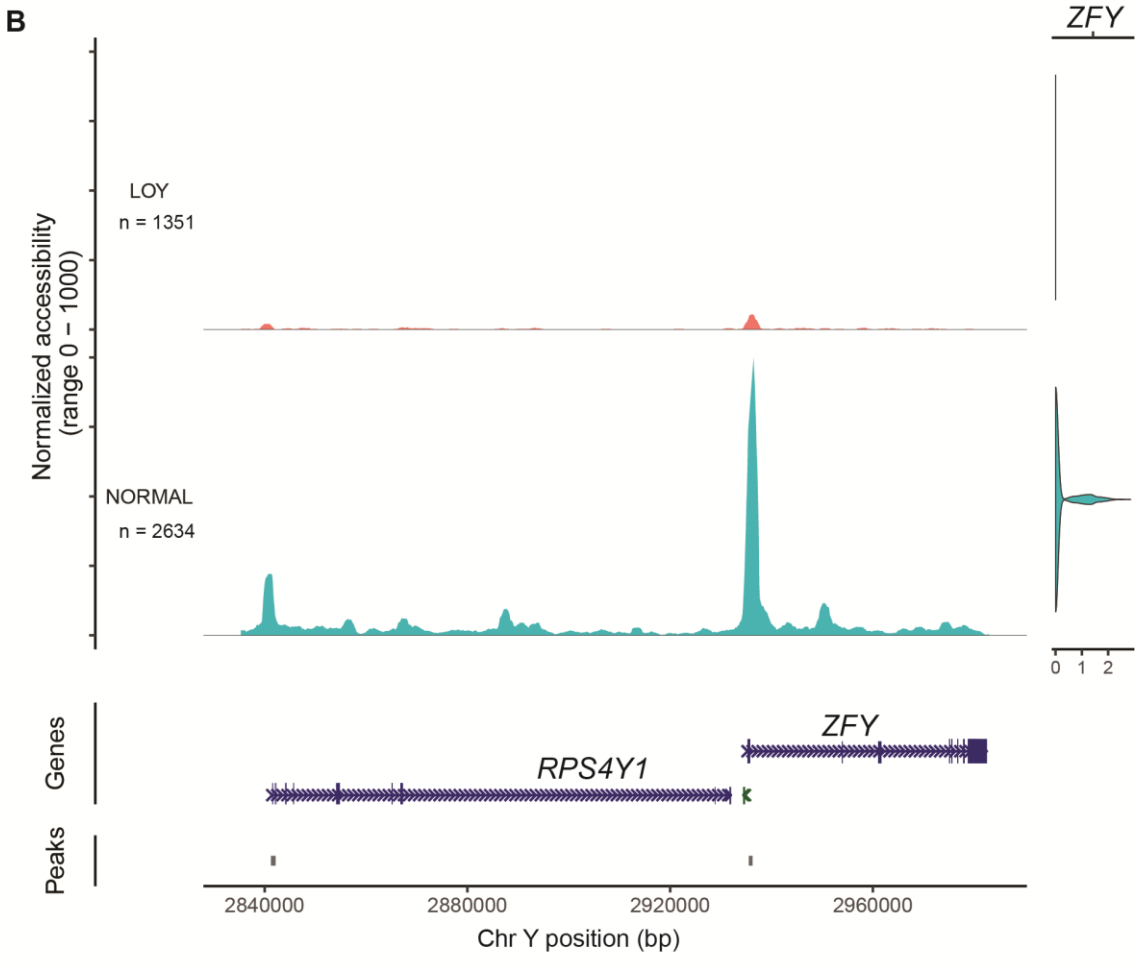
B
ZFY
LOY
n = 1351
NORMAL
n = 2634
Normalized accessibility
(range 0 – 1000)
0 1 2
Genes
ZFY
RPS4Y1
Peaks
2840000
2880000
2920000
2960000
Chr Y position (bp)

Supplemental Figure S3: Visualization of chromatin accessibility and gene expression in LOY nuclei for two MSY genes (*UTY* and *ZFY*). Multi-modal coverage plots showing chromatin accessibility and gene expression data for LOY and non-LOY/normal nuclei for two MSY genes (*A*) *UTY* and (*B*) *ZFY*. In each panel the top shows normalized chromatin accessibility peaks for LOY and normal nuclei, which correspond with the genomic coordinates (hg38) and gene model at the bottom. The right panel contains violin plots of normalized gene expression for the gene of interest. LOY was classified using snRNA-seq and was determined by the absence of all MSY gene expression. All included nuclei were filtered using gene expression and ATAC sequencing metrics which included: >1500 UMI counts, >1000 features (GEX), and >10000 UMI counts, >1000 features (ATAC).

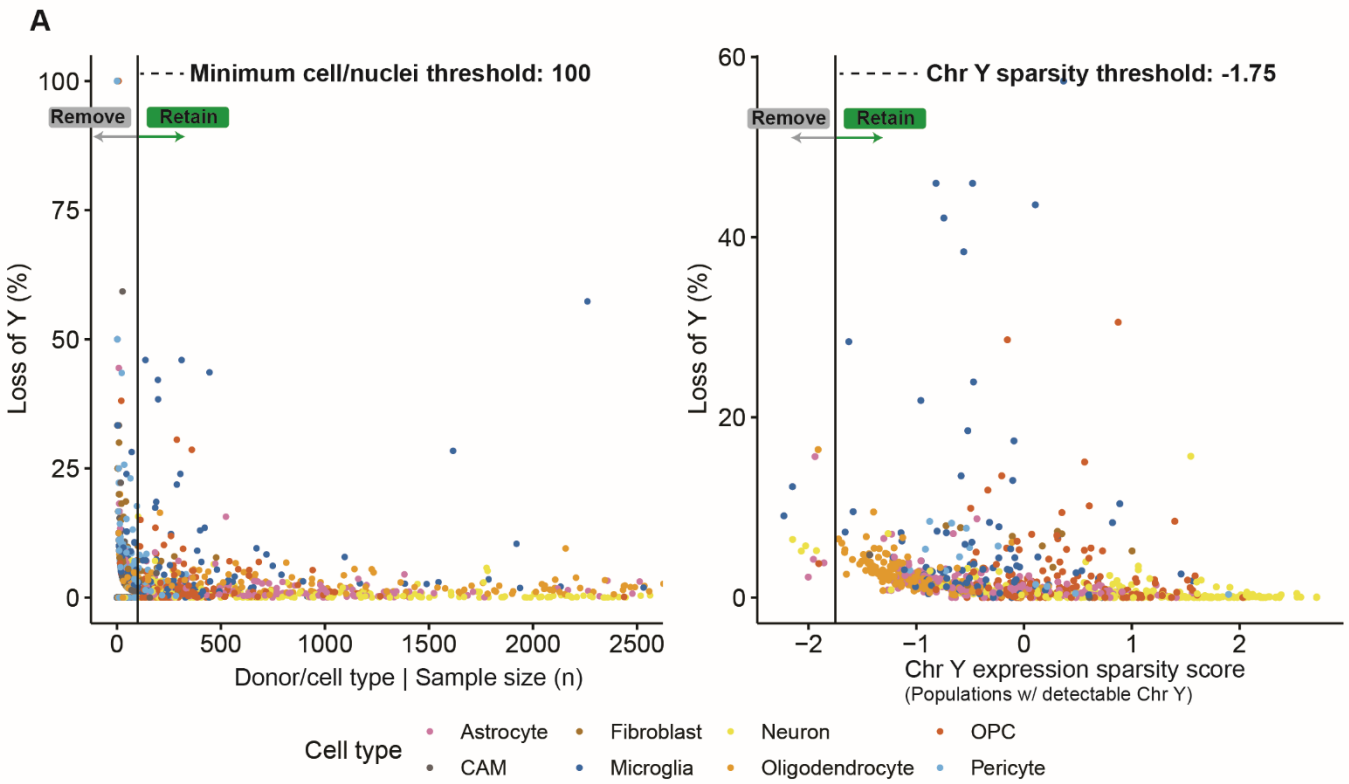

Supplemental Figure S4: QC threshold values for sample size and MSY sparsity score. Scatterplots displaying quality control threshold values for (*A*) cell/nuclei population sample size and (*B*) MSY sparsity score (in Chr Y proficient/Chr Y wt cells). Each point represents a donor/cell type population and is colored by labelled cell type. Each donor/cell type population required >= 100 cells/nuclei and >= -1.75 MSY sparsity score to be included in LOY proportion estimation. More information on MSY sparsity score can be found in **Supplemental Fig. S7**, **Supplemental Methods** and **Supplemental Code**.

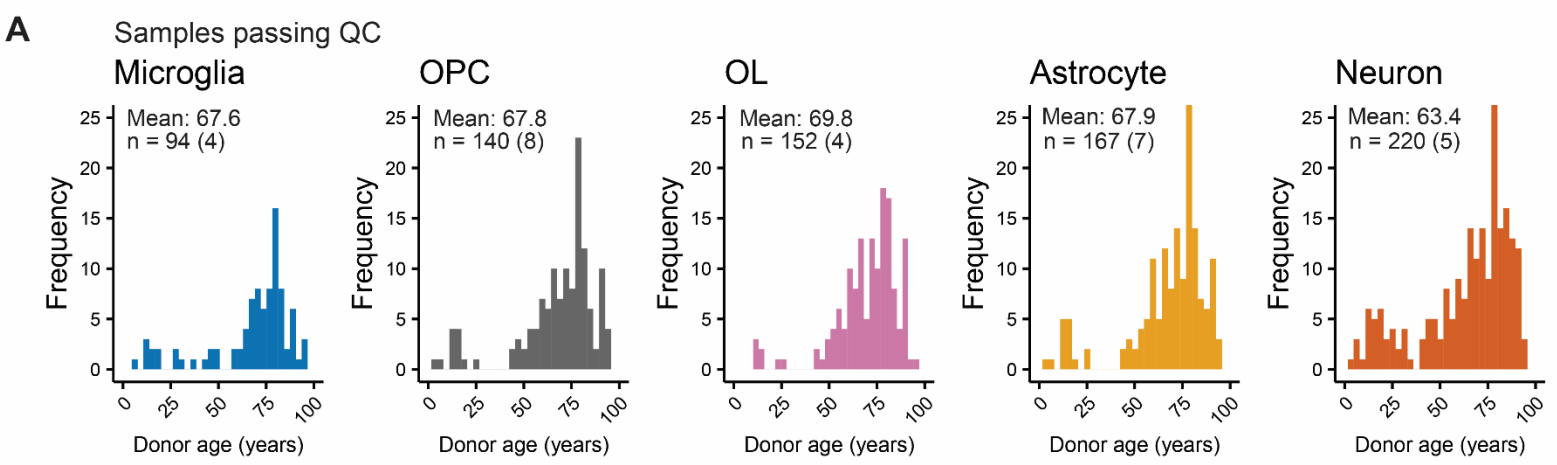

Supplemental Figure S5: Donor age distribution for each brain cell type population. Included donor/cell type populations required >= 100 cells/nuclei (>=3000 UMI; >=1000 Genes) and >-1.75 MSY sparsity score (**Supplemental Methods**; **Supplemental Fig. S7**). Mean donor age and sample size for each cell type are provided at the top of each histogram. The total number of QC passing donors without age data is provided in parentheses. Samples lacking age data were not included in analyses involving age adjustment.

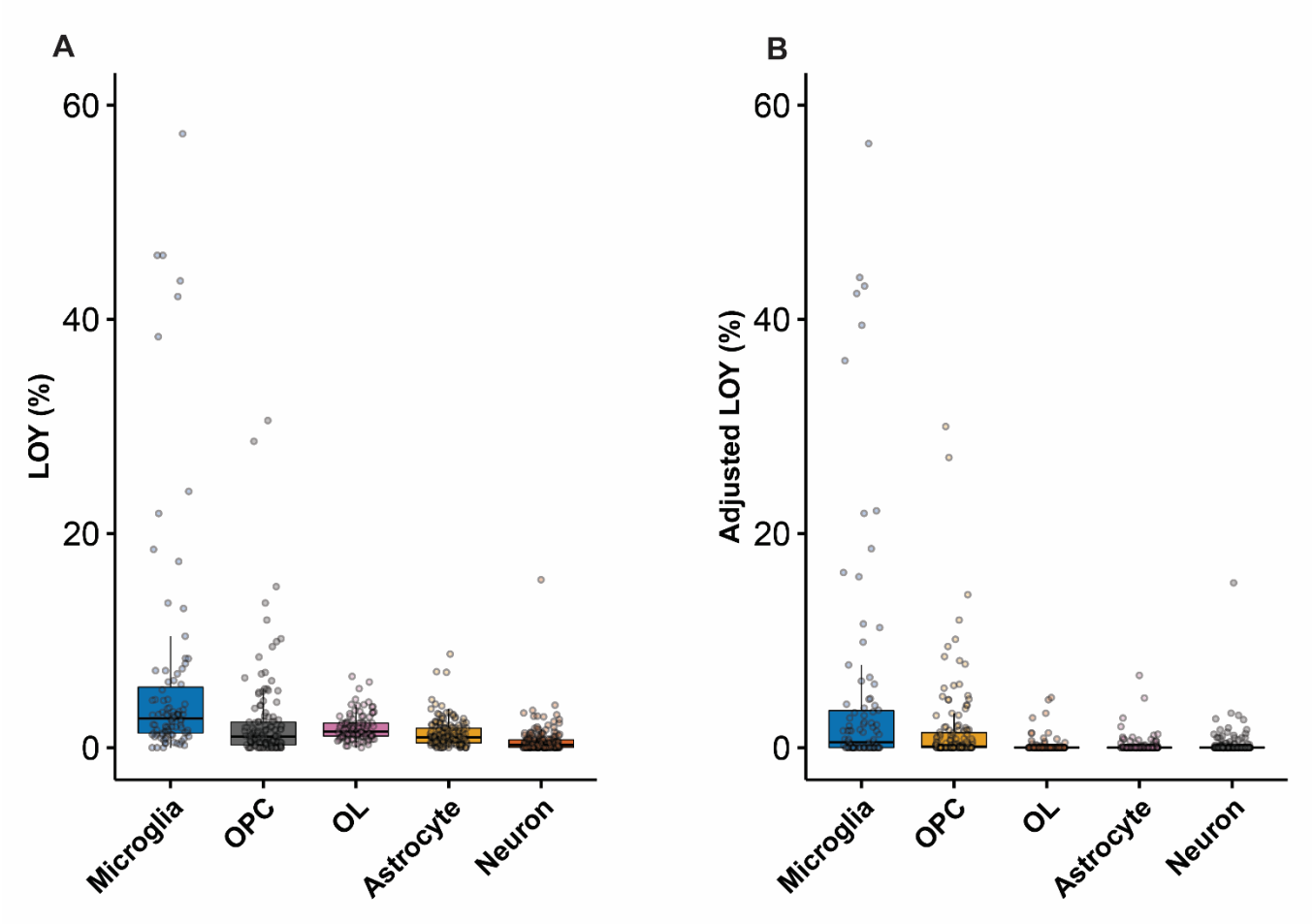

Supplemental Figure S6: Effect of MSY sparsity adjustment for each major brain cell type. Boxplots of mean LOY frequencies of each donor across brain cell types using (*A*) unadjusted and (*B*) adjusted LOY estimates. LOY enrichment was observed in microglia populations before and after adjustment using MSY sparsity (**Supplemental Fig. S7**). In oligodendrocytes and astrocytes MSY expression was often sparse and lacked feature diversity. For this reason, oligodendrocyte and astrocyte LOY estimation is often inflated when using raw values but is corrected after MSY sparsity adjustment.

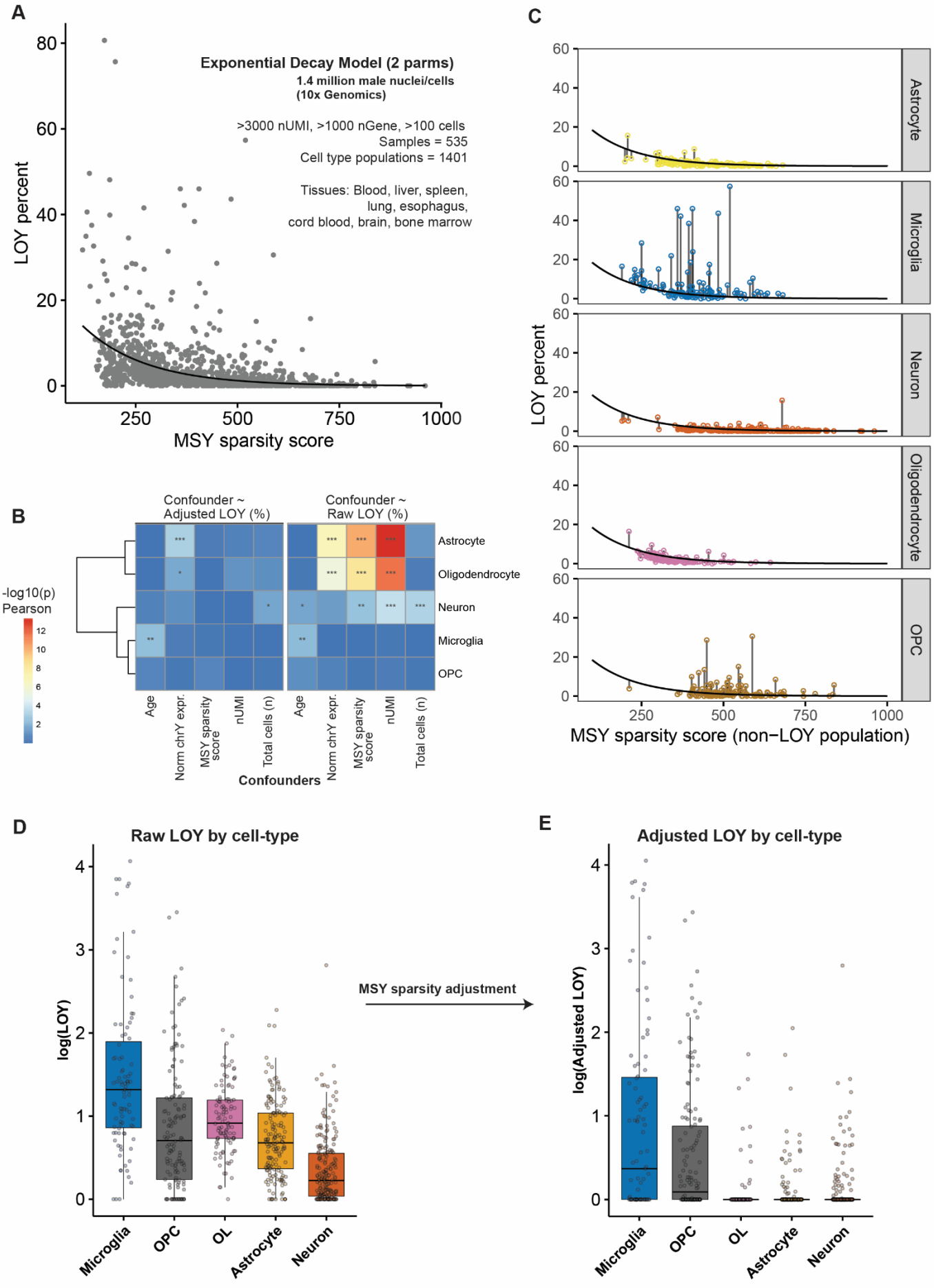
A
Exponential Decay Model (2 parms)
1.4 million male nuclei/cells
(10x Genomics)
>3000 nUMI, >1000 nGene, >100 cells
Samples = 535
Cell type populations = 1401
Tissues: Blood, liver, spleen, lung, esophagus, cord blood, brain, bone marrow
LOY percent
MSY sparsity score
B
Confounder ~ Adjusted LOY (%)
Confounder ~ Raw LOY (%)
-log10(p) Pearson
Astrocyte
Oligodendrocyte
Neuron
Microglia
OPC
Age
Norm chrY expr.
MSY sparsity score
nUMI
Total cells (n)
Confounders
C
LOY percent
MSY sparsity score (non−LOY population)
D
Raw LOY by cell-type
log(LOY)
Microglia
OPC
OL
Astrocyte
Neuron
MSY sparsity adjustment
E
Adjusted LOY by cell-type
log(Adjusted LOY)

Supplemental Figure S7: Adjusting LOY values using MSY gene sparsity. Summary of LOY adjustment strategy using MSY sparsity. (*A*) A 2-parameter exponential decay model was fit to LOY percentage and MSY sparsity using data from single-cell and single-nuclei data (droplet-based 10x Genomics) (**Supplemental Data S1**; **Supplemental Code**). Single-cell data included 535 donors and was derived from brain, blood, liver, spleen, lung, esophagus, cord blood, and bone marrow. All primary tumor samples were removed. (*B*) Heatmap showing Pearson correlations between LOY percentage and technical confounders before (*Right*) and after (*Left*) MSY sparsity adjustment. Pearson correlation: (*ns*) $P > 0.05$, (*) $P < 0.01$, (**) $P < 0.001$, (***) $P < 0.0001$. (*C*) To determine adjusted LOY estimates, our brain data was fit to the decay model and residuals were retained. Positive residuals were set as adjusted LOY estimates. Donor/cell types with negative residuals were given adjusted LOY values of 0. (*D-E*) Boxplots displaying the log transformed (*D*) raw LOY estimates and (*E*) MSY sparsity adjusted LOY estimates.

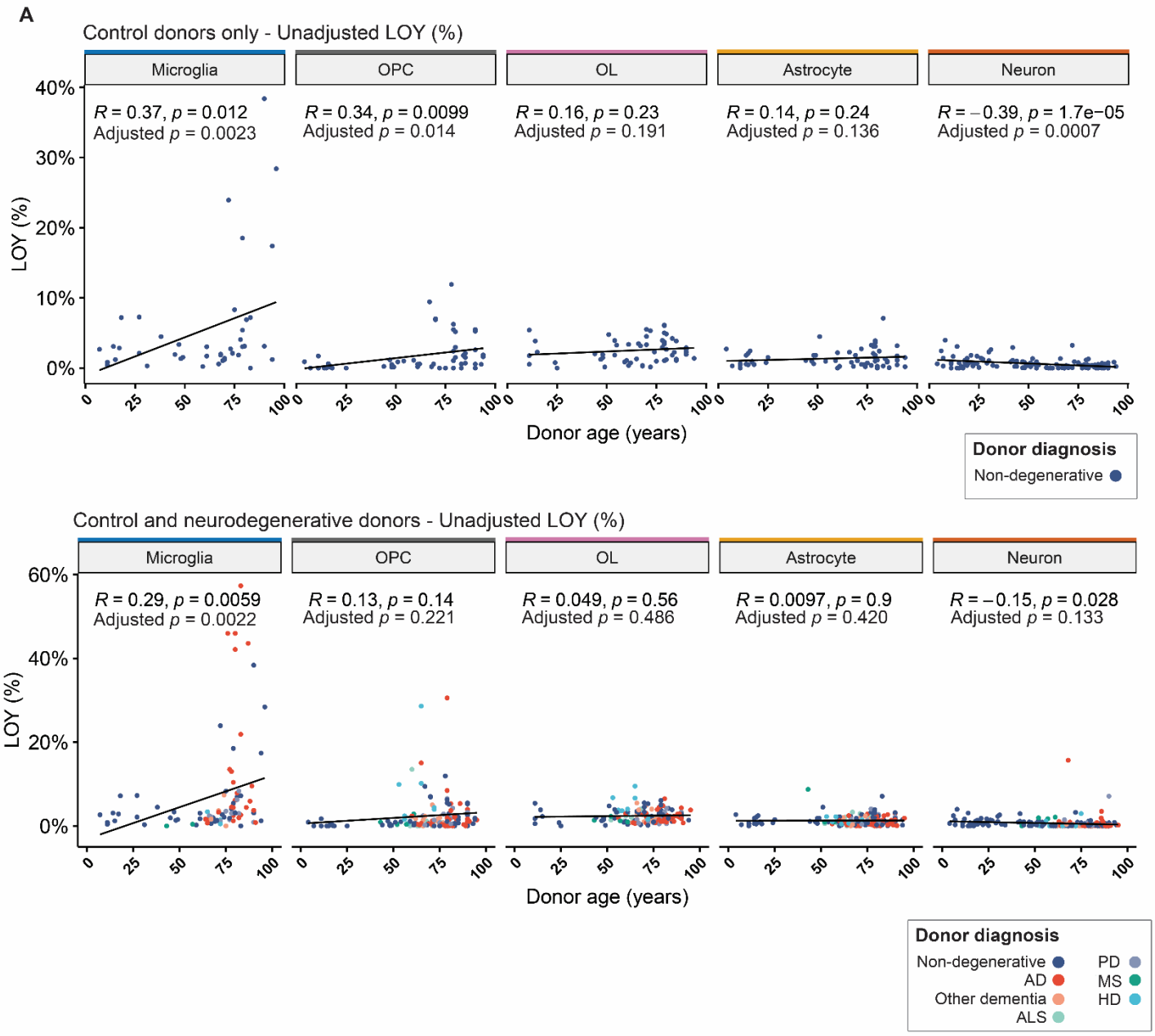

Supplemental Figure S8A: Cell type–specific associations between LOY estimates and age. Scatterplots displaying the correlation between unadjusted LOY percentage and age for control donors (*Top*) and all donors (*Bottom*) across five major brain cell types. Points represent an individual donor/cell type population and are colored based on neurological diagnosis. Each scatter plot contains a linear model with the formula: LOY ~ Donor age. The associated Pearson correlation and *p*-value are provided in the first line of each header. Adjusted *p*-values are derived from a multiple linear regression model with the formula: LOY ~ median_nUMI + 10x chemistry + MSY sparsity score + donor_organism.age.

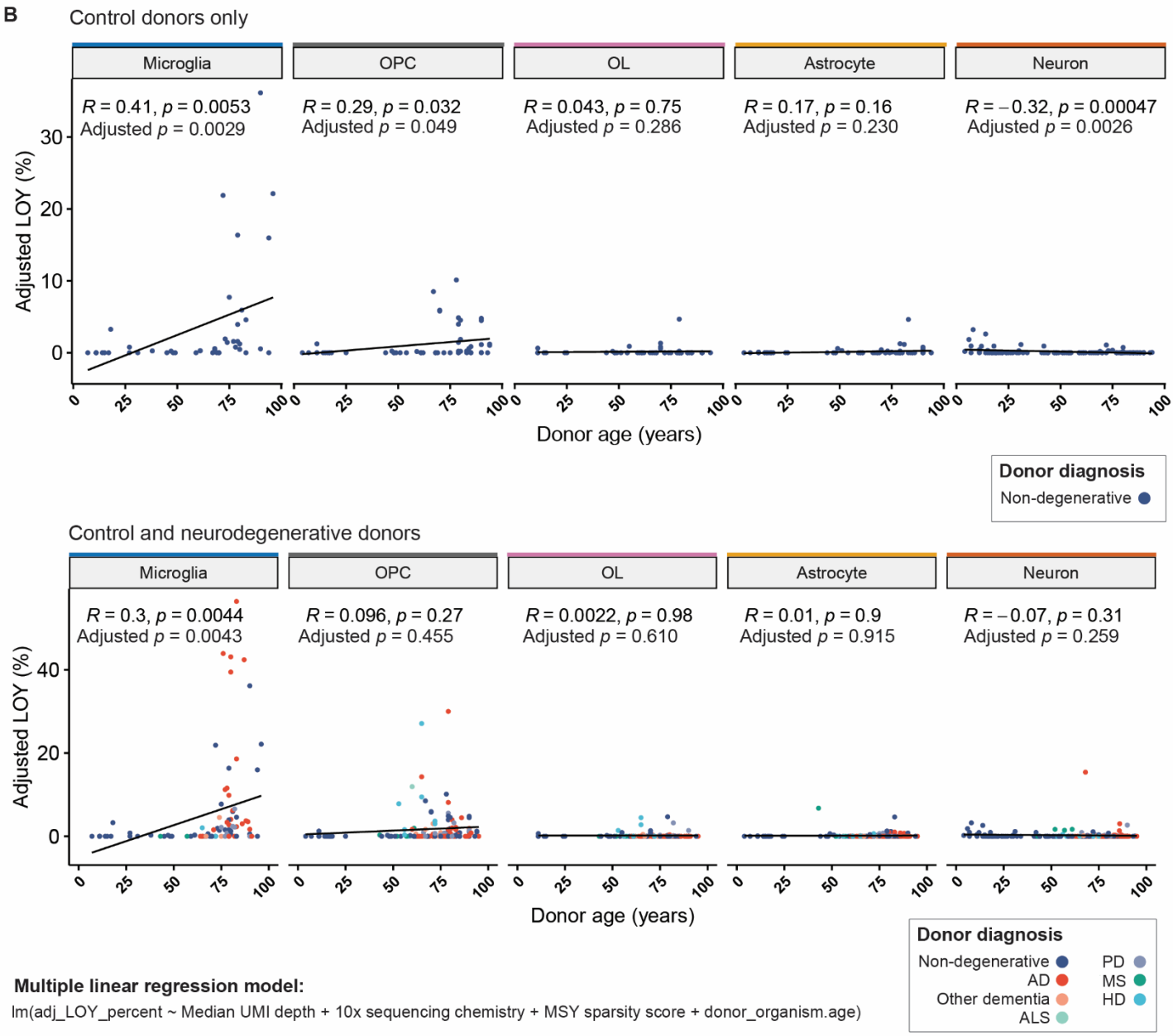

Supplemental Figure S8B: Cell type–specific associations between LOY estimates and age. Scatterplots displaying the correlation between adjusted LOY percentage and age in control donors (*Top*) and all donors (*Bottom*) across five major brain cell types. Points represent an individual donor/cell type population and are colored based on neurological diagnosis. LOY estimates were adjusted using MSY sparsity scores (**Methods**). Each scatter plot contains a linear model with the formula: LOY ~ Donor age. The associated Pearson correlation and *p*-value are provided in the first line of each header. Adjusted *p*-values are derived from a multiple linear regression model with the formula: LOY ~ median_nUMI + 10x chemistry + MSY sparsity score + donor_organism.age.

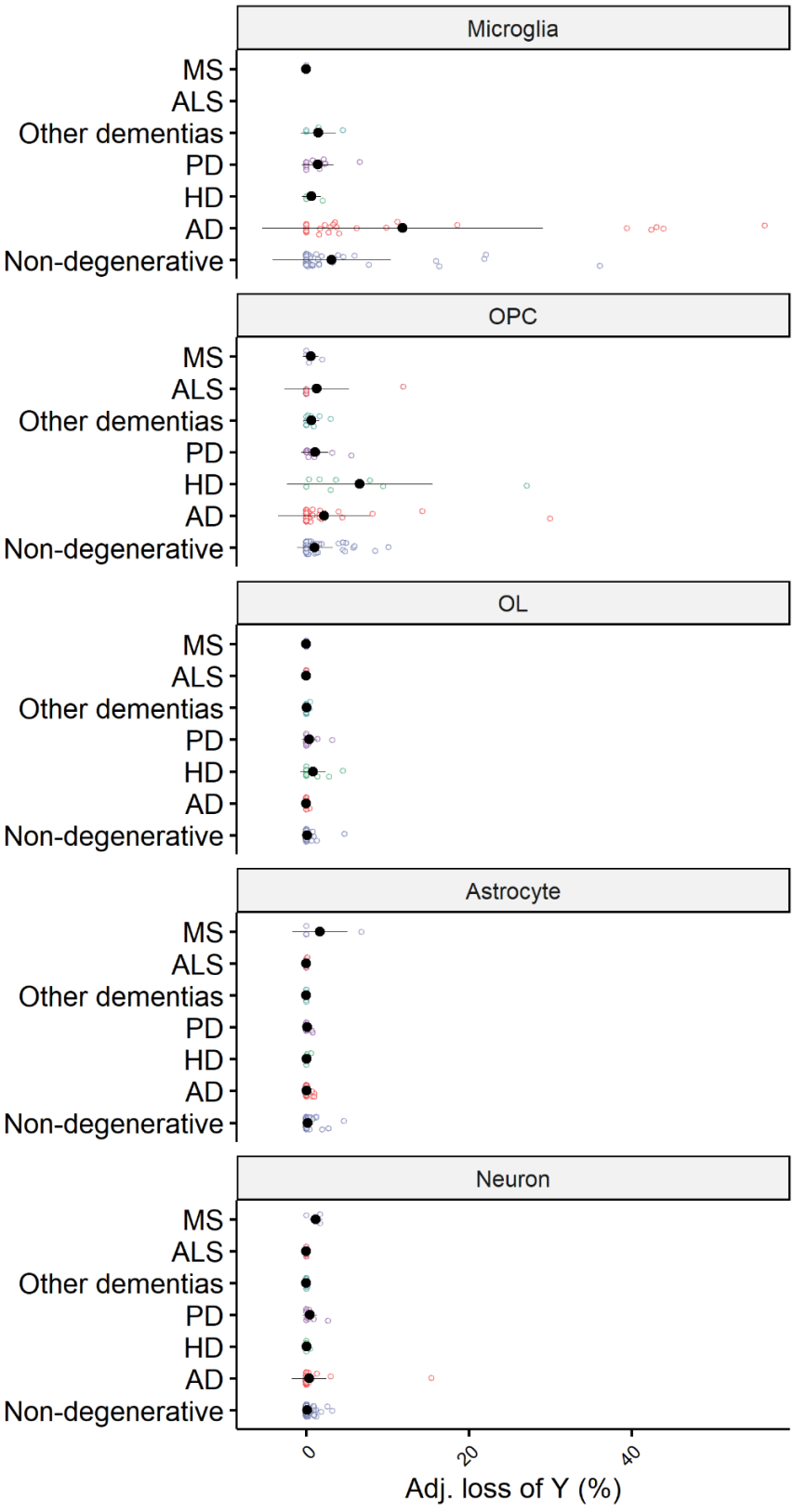

Supplemental Figure S9: Disease–specific LOY across five major brain cell types. LOY frequencies facetted by neurodegerative diagnosis and brain cell type. Black points represent median LOY frequency, while black lines represent the interquartile range. Each colored point represents the LOY percentage estimate of a cell type population in an individual donor.

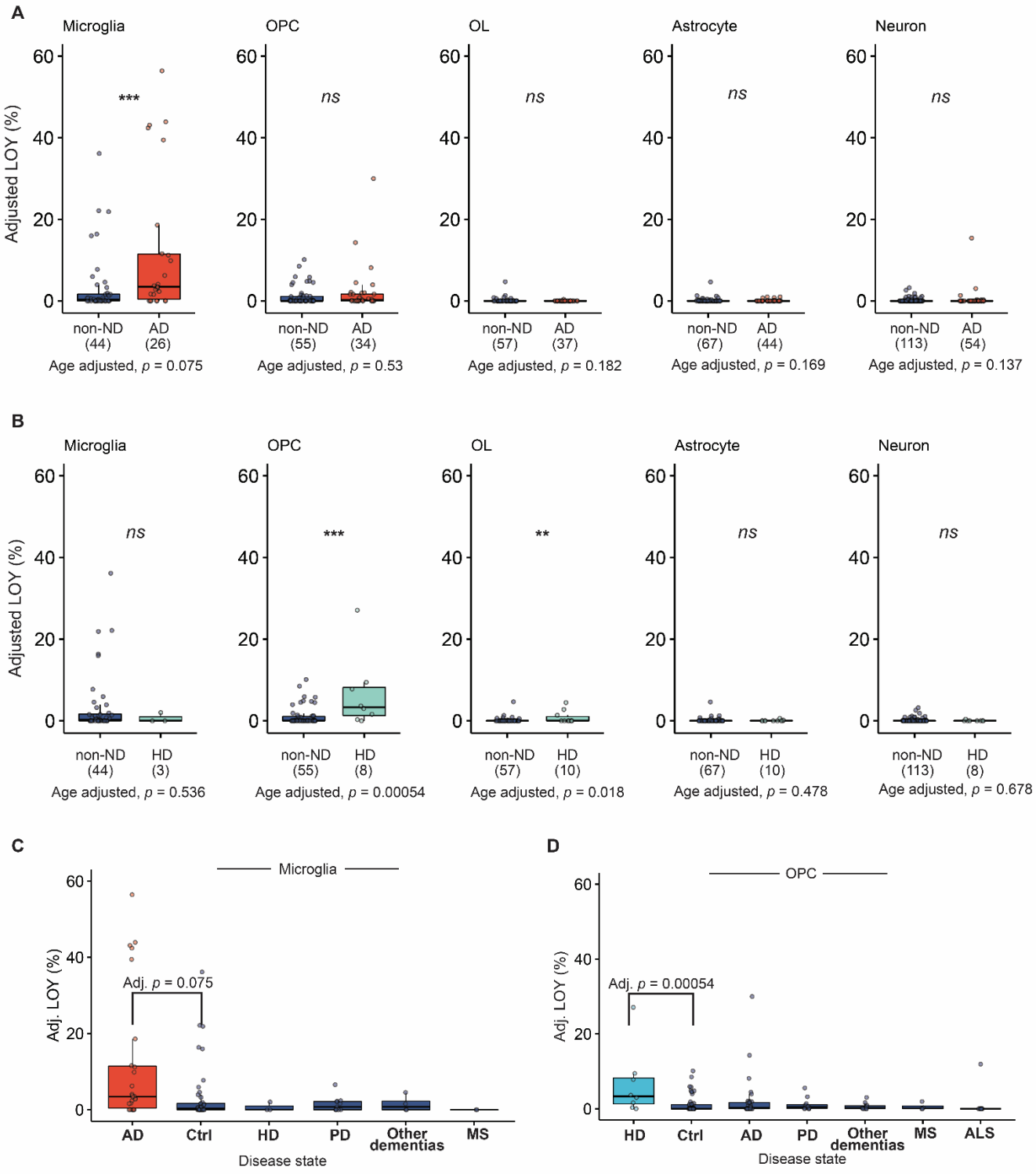

Supplemental Figure S10: Comparing LOY estimates between AD, HD and control donors. (*A*,*B*) LOY percentage estimates between (*A*) AD or (*B*) HD and control donors for each major brain cell type. Non-neurodegerative (Non-ND) refers to donors without a neurodegerative diagnosis. Adjusted *P*-values are derived from a multiple linear regression model with the formula: LOY ~ median_nUMI + 10x chemistry + MSY sparsity score + donor_organism.age + diagnosis. Donor sample size for each group is provided in parenthesis on the *x*-axis. (*C*,*D*) Boxplots displaying adjusted LOY percentages in for (*C*) microglia and (*D*) OPCs between control, AD and other neurodegerative diseases.

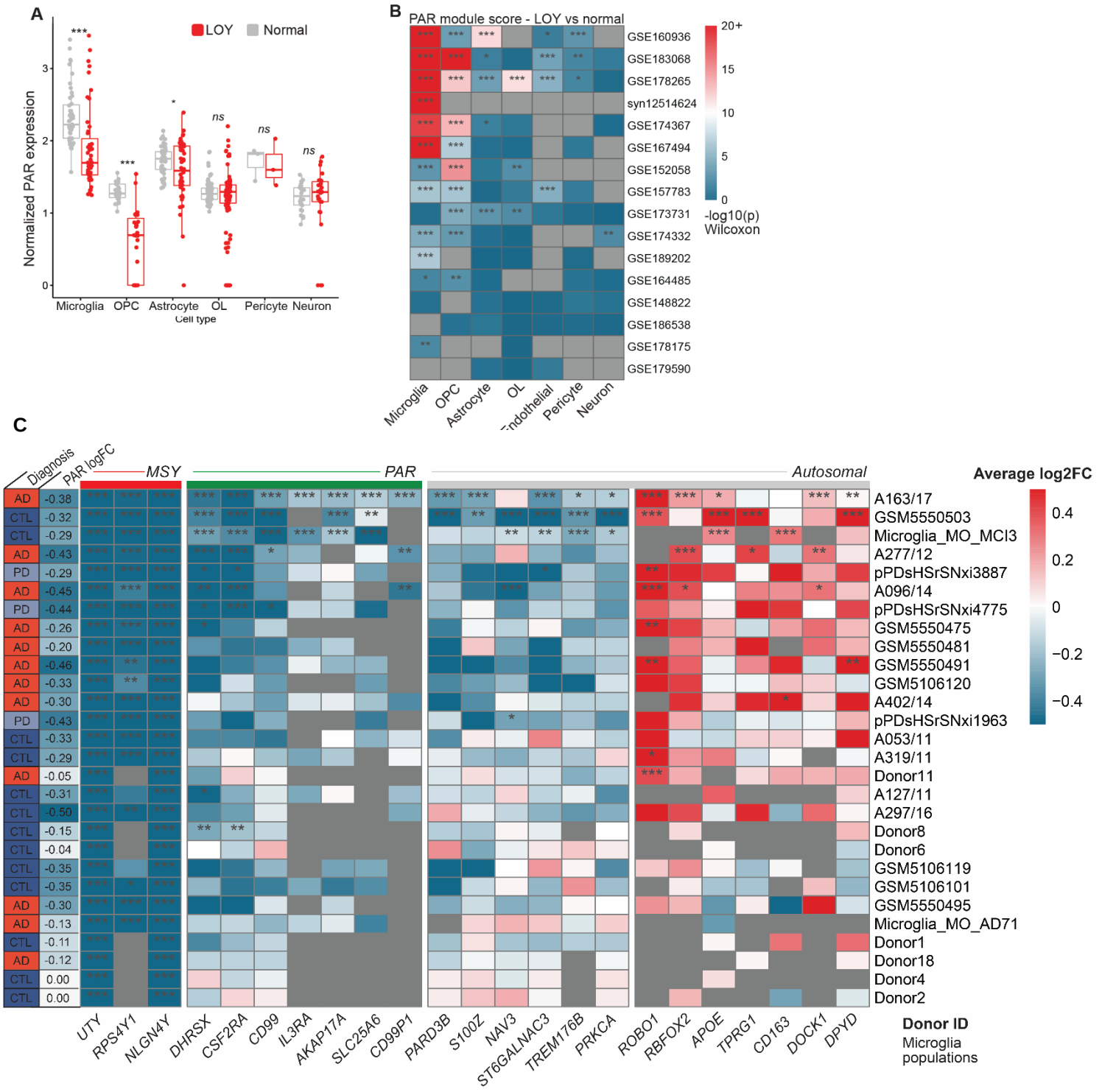

Supplemental Figure S11: Cumulative PAR and mLATE gene expression across 28 donors (*A*) Cumulative, normalized PAR expression compared between LOY and normal population for each major brain cell type. Each point represents an individual donor population with > 25 cells (Paired Wilcoxon test) (*C*) Heatmap showing significance of PAR expression loss between LOY and normal populations within each brain cell type across 16 cohorts. Significance values were determined using Wilcoxon tests between PAR module scores for all LOY and normal nuclei in each group. Populations with > 25 cells were included. Wilcoxon test: (*ns*) $P > 0.05$; (*) $P < 0.05$, (**) $P < 0.01$, (***) $P < 0.001$. (*B*) Heatmap illustrating microglia DE (average logFC) for individual subjects with > 50 LOY cells/nuclei. Additional columns on the left show cumulative PAR expression and neurodegerative diagnosis, respectively. Significance is provided within each cell. False-discovery rate: (*) FDR < 0.05, (**) FDR < 0.01, (***) FDR < 0.001.

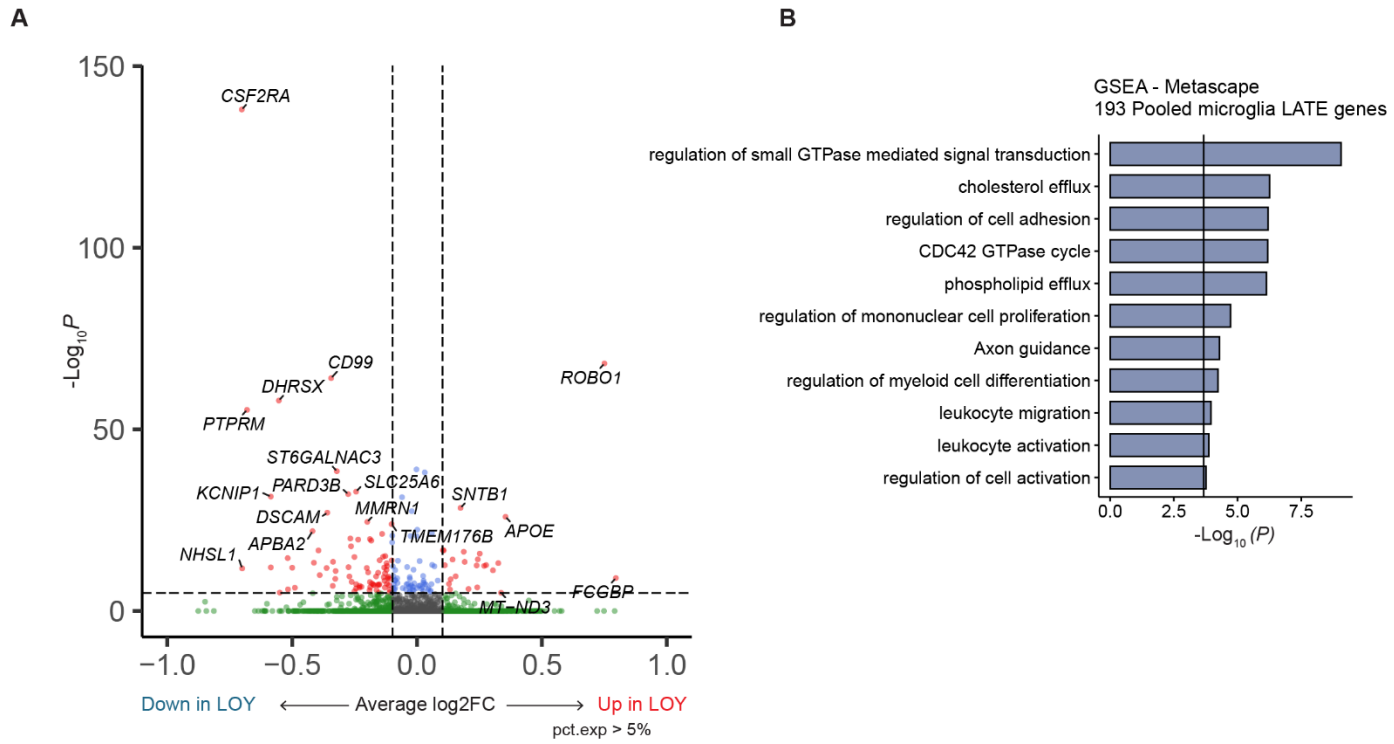

Supplemental Figure S12: Differential expression analysis in pooled microglia between LOY and normal single-cell populations. (*A*) Volcano plot showing 193 differentially expressed genes in LOY microglia (Bonferroni, $P < 0.1$ & abs(logFC) > 0.10). LOY was classified using Chr Y genes so all male-specific Y genes were removed from visualization. The following 19 samples were included in this analysis: GSM4886748, GSM4886749, GSM4886750, GSM4886751, GSM4886758, GSM4886760, GSM4886761, GSM5106119, GSM5106120, GSM5550451, GSM5550475, GSM5550481, GSM5550491, GSM5550495, GSM5550501, GSM5550503, Microglia_MO_MCI3, pPDsHSrSNxi1963, pPDsHSrSNxi4775. DE genes were called using MAST with latent variables including sample, nUMI, nFeature, and percent.mt. (*B*) Enriched gene sets for 193 mLATE genes from Metascape ($P < 0.05$; Bonferroni) (**Supplemental Table S5**)

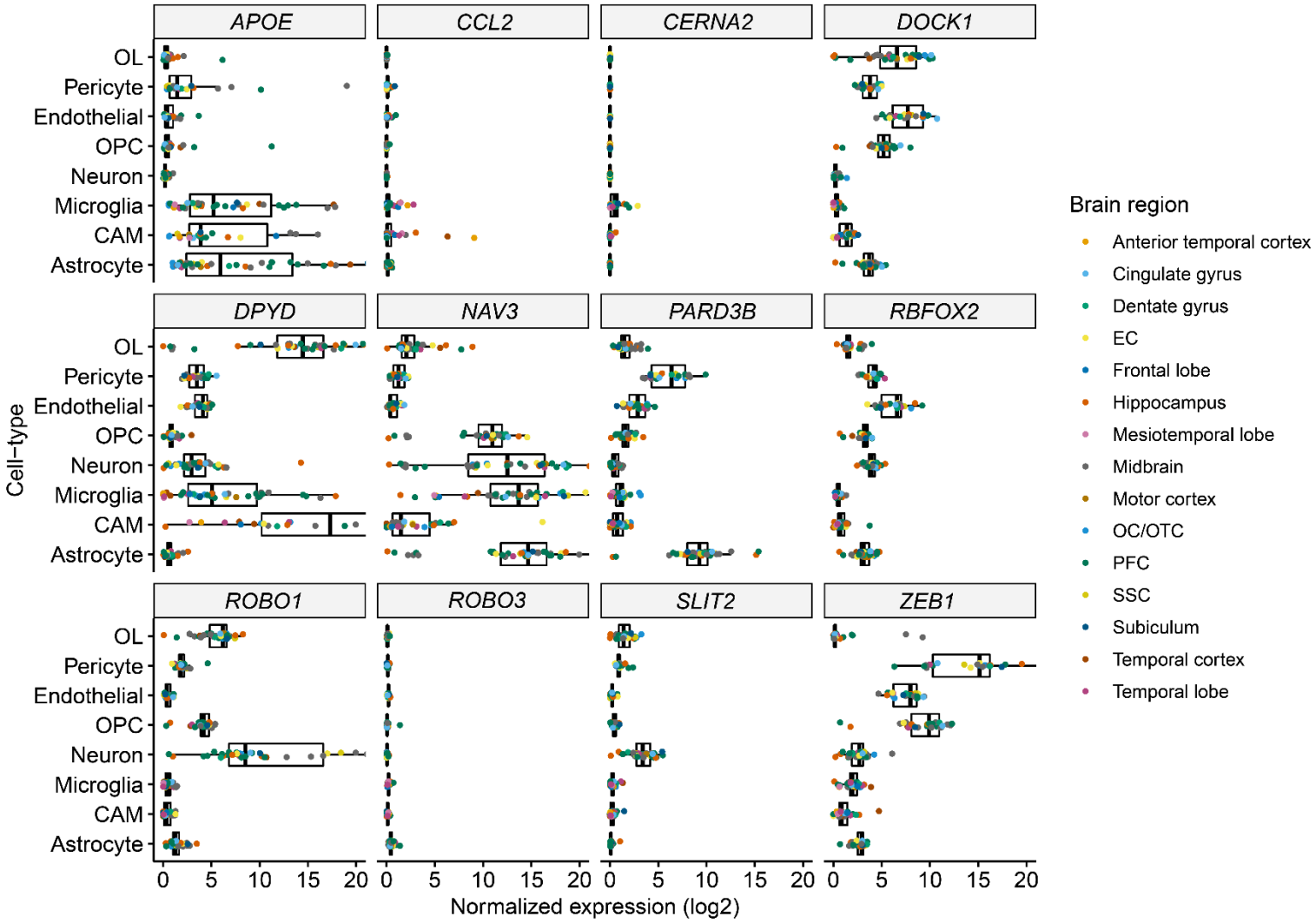

Supplemental Figure S13: Expression of recurrent microglia LOY DE genes and SLIT/ROBO genes across all brain cell types. Boxplots illustrate cell type–specific expression of selected mLATE, SLIT/ROBO signaling pathway genes and infiltrating monocyte marker genes (*CCL2*). Points overlayed on each boxplot are colored by sample brain region origin. OL Oligodendrocyte, CAM CNS-associated macrophage, OPC oligodendrocyte progenitor cell, EC Entorhinal cortex, OC Occipital cortex, OTC Occipitotemporal cortex, PFC Pre-frontal cortex, SSC Somatosensory cortex.

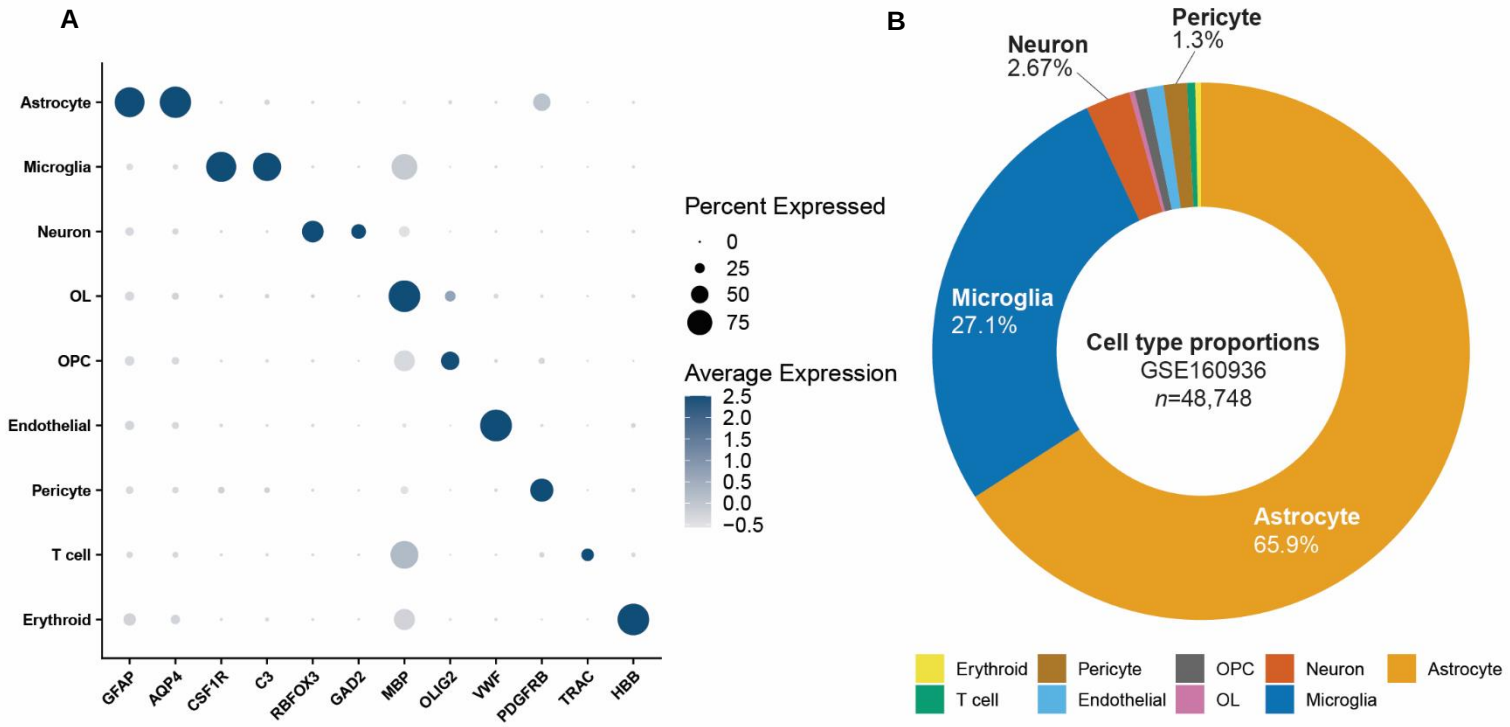

Supplemental Figure S14: Cell type marker genes and proportions for GSE160936 single-nuclei dataset from AD and control brain tissue. Corresponds to Figure 4. (*A*) Dot plot displaying markers genes used to annotate Leiden clusters with cell types. (*B*) Donut chart of relative cell type proportions (n = 48,748). Astrocytes and microglia nuclei clusters represent over 90% of all nuclei in from the GSE160936 dataset.

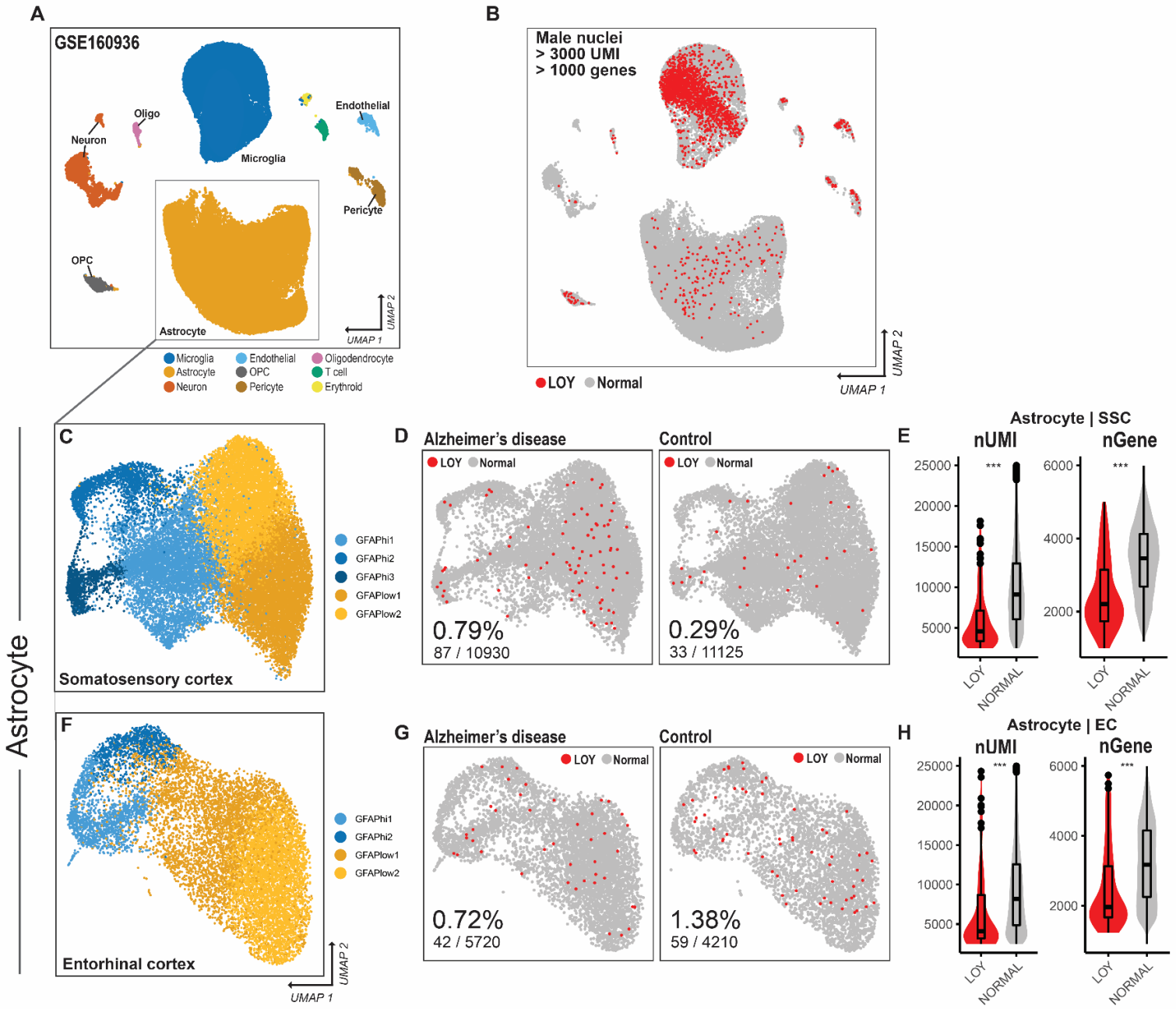

Supplemental Figure S15: LOY frequencies in astrocytes across the EC and SSC (GSE160936). (*A*) UMAP reduction and cell type annotations of 48,748 single-nuclei brain transcriptomes from GSE160936. Markers used to annotate clusters include *C3* and *CSF1R* (microglia), *AQP4* and *GFAP* (astrocyte), *RBFOX3* and *GAD1* (neuron), and *MBP* (oligodendrocyte). (*B*) UMAP plot showing LOY classification of each male nucleus (nUMI > 3000 and nGene > 1000). LOY nuclei (red) and non-LOY/normal nuclei (grey). Astrocyte nuclei from SSC (*C*) and EC (*F*) were isolated, CCA integrated, and clustered. (*C*,*F*), Subclusters were annotated using high (yellows) and low (blues) *GFAP* expression. (*D*,*G*), UMAP reductions of SSC and EC split by AD diagnosis; Nuclei are colored by LOY (red) and non-LOY/normal (grey). LOY nuclei frequencies are provided at the bottom of each UMAP plot. (*E*,*H*), Violin boxplots showing UMI counts (nUMI) and detected genes (nGenes) for LOY and normal nuclei. The boxes represent the 25th percentile, median, and 75th percentile. The whiskers extend to the furthest value that is no more than 1.5 times the inter-quartile range. Significant differences between LOY and non-LOY groups were assessed using the non-parametric Wilcoxon test, resulting in the p-values shown for each comparison. All tests were two-sided. *ns* < 0.05, *P* > 0.05, **P* < 0.05, ***P* < 0.01, ****P* < 0.001.

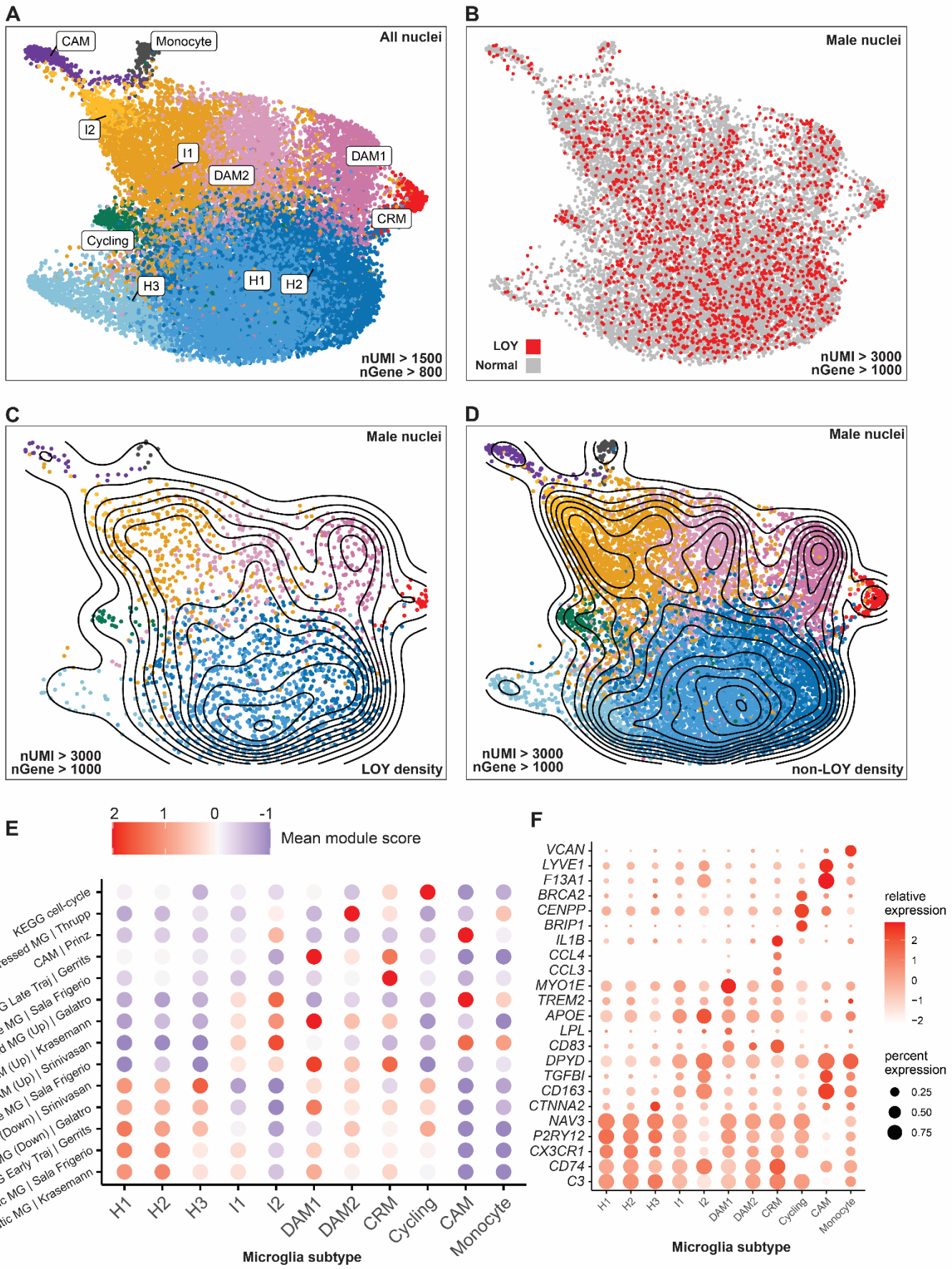
A
All nuclei
CAM
Monocyte
I2
I1
DAM2
DAM1
CRM
Cycling
H3
H1
H2
nUMI > 1500
nGene > 800
B
Male nuclei
LOY
Normal
nUMI > 3000
nGene > 1000
C
Male nuclei
nUMI > 3000
nGene > 1000
LOY density
D
Male nuclei
nUMI > 3000
nGene > 1000
non-LOY density
E
2
1
0
-1
Mean module score
KEGG cell-cycle
Stressed MG | Thrupp
CAM | Prinz
AD MG Late Traj | Gerrits
Cytokine response MG | Sala Frigerio
Age-associated MG (Up) | Galatro
DAM (Up) | Krasemann
HAM (Up) | Srinivasan
Activated response MG | Sala Frigerio
HAM (Down) | Srinivasan
Age-associated MG (Down) | Galatro
AD MG Early Traj | Gerrits
Homeostatic MG | Sala Frigerio
Homeostatic MG | Krasemann
H1
H2
H3
I1
I2
DAM1
DAM2
CRM
Cycling
CAM
Monocyte
Microglia subtype
F
VCAN
LYVE1
F13A1
BRCA2
CENPP
BRIP1
IL1B
CCL4
CCL3
MYO1E
TREM2
APOE
LPL
CD83
DPYD
TGFBI
CD163
CTNNA2
NAV3
P2RY12
CX3CR1
CD74
C3
relative expression
2
1
0
−1
−2
percent expression
0.25
0.50
0.75
H1
H2
H3
I1
I2
DAM1
DAM2
CRM
Cycling
CAM
Monocyte
Microglia subtype

Supplemental Figure S16A: Microglia subtype characterization and LOY summary (GSE160936). Microglia from single-nuclei RNAseq data (10x 3' v3) from GEO accession GSE160936 were isolated and reprocessed. (*A*) UMAP plot showing microglia subtype clusters for 15,791 male and 7,040 female nuclei. Each point represents a nuclei transcriptome and is coloured by subtype annotation (nUMI > 1500 & nGene > 800). (*B*) UMAP plot illustrating LOY status for each included male microglia (LOY: 15.9%; *n* = 1942; nUMI > 3000; nGene > 1000). (*C*-*D*) Density contours for (*C*) LOY nuclei and (*D*) non-LOY nuclei illustrate clustering density patterns for each group. (*E*-*F*) Heatmaps displaying (*E*) published microglia gene set module scores and (*F*) marker genes/DE genes used to annotate each subcluster. Gene sets used are provided in **Supplemental Table S8**. H1-3 Homeostatic microglia, DAM1-2 Disease associated microglia, I1-2 Inflammatory microglia, CRM Cytokine release microglia.

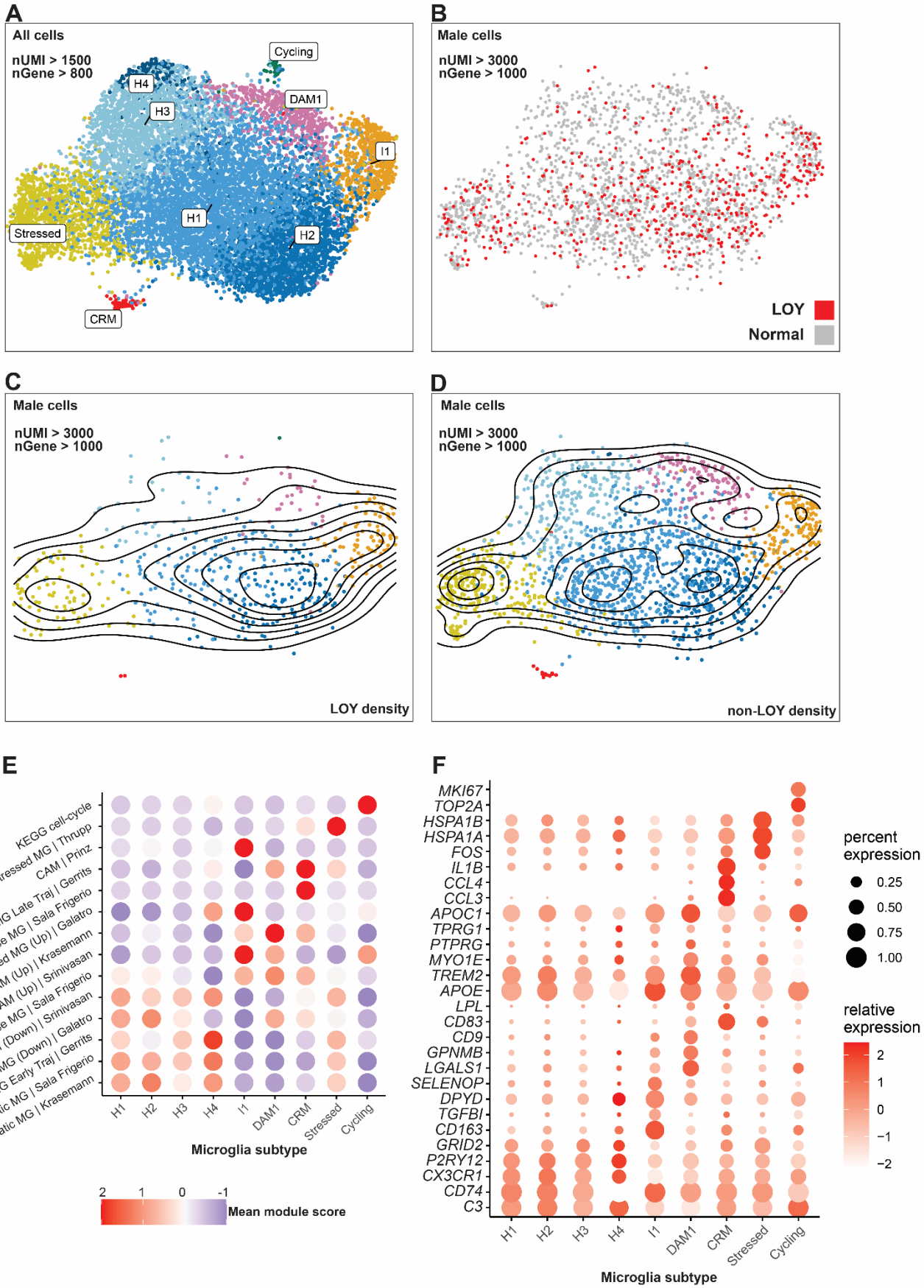
A
All cells
nUMI > 1500
nGene > 800
Cycling
H4
DAM1
H3
I1
H1
H2
Stressed
CRM
B
Male cells
nUMI > 3000
nGene > 1000
LOY
Normal
C
Male cells
nUMI > 3000
nGene > 1000
LOY density
D
Male cells
nUMI > 3000
nGene > 1000
non-LOY density
E
KEGG cell-cycle
Stressed MG | Thrupp
CAM | Prinz
AD MG Late Traj | Gerrits
Cytokine response MG | Sala Frigerio
Age-associated MG (Up) | Galatro
DAM (Up) | Krasemann
HAM (Up) | Srinivasan
Activated response MG | Sala Frigerio
HAM (Down) | Srinivasan
Age-associated MG (Down) | Galatro
AD MG Early Traj | Gerrits
Homeostatic MG | Sala Frigerio
Homeostatic MG | Krasemann
H1
H2
H3
H4
I1
DAM1
CRM
Stressed
Cycling
Microglia subtype
2
1
0
-1
Mean module score
F
MKI67
TOP2A
HSPA1B
HSPA1A
FOS
IL1B
CCL4
CCL3
APOC1
TPRG1
PTPRG
MYO1E
TREM2
APOE
LPL
CD83
CD9
GPNMB
LGALS1
SELENOP
DPYD
TGFBI
CD163
GRID2
P2RY12
CX3CR1
CD74
C3
H1
H2
H3
H4
I1
DAM1
CRM
Stressed
Cycling
Microglia subtype
percent expression
0.25
0.50
0.75
1.00
relative expression
2
1
0
−1
−2

Supplemental Figure S16B: Microglia subtype characterization and LOY summary (syn12514624). Microglia from single-cell RNAseq data (10x 3' v2) from Synapse accession syn12514624 were isolated and reprocessed. (*A*) UMAP plot showing microglia subtype clusters for male (n = 4,580) and female (n = 6,741) nuclei. Each point represents a nucleus and is coloured by subtype annotation (nUMI > 1500 & nGene > 800). (*B*) UMAP plot illustrating LOY status for each included male microglia (LOY %: 22.7%; nUMI > 3000 & nGene > 1000). (*C*-*D*) Density contours for (*C*) LOY nuclei and (*D*) non-LOY nuclei illustrate clustering density patterns for each group. (*E*-*F*) Heatmaps displaying (*E*) published microglia gene set module scores and (*F*) marker genes/DE genes used to annotate each subcluster. Gene sets used are provided in **Supplemental Table S8**. H1-4 Homeostatic microglia, DAM1 Disease associated microglia, I1 Inflammatory microglia, CRM Cytokine release microglia.

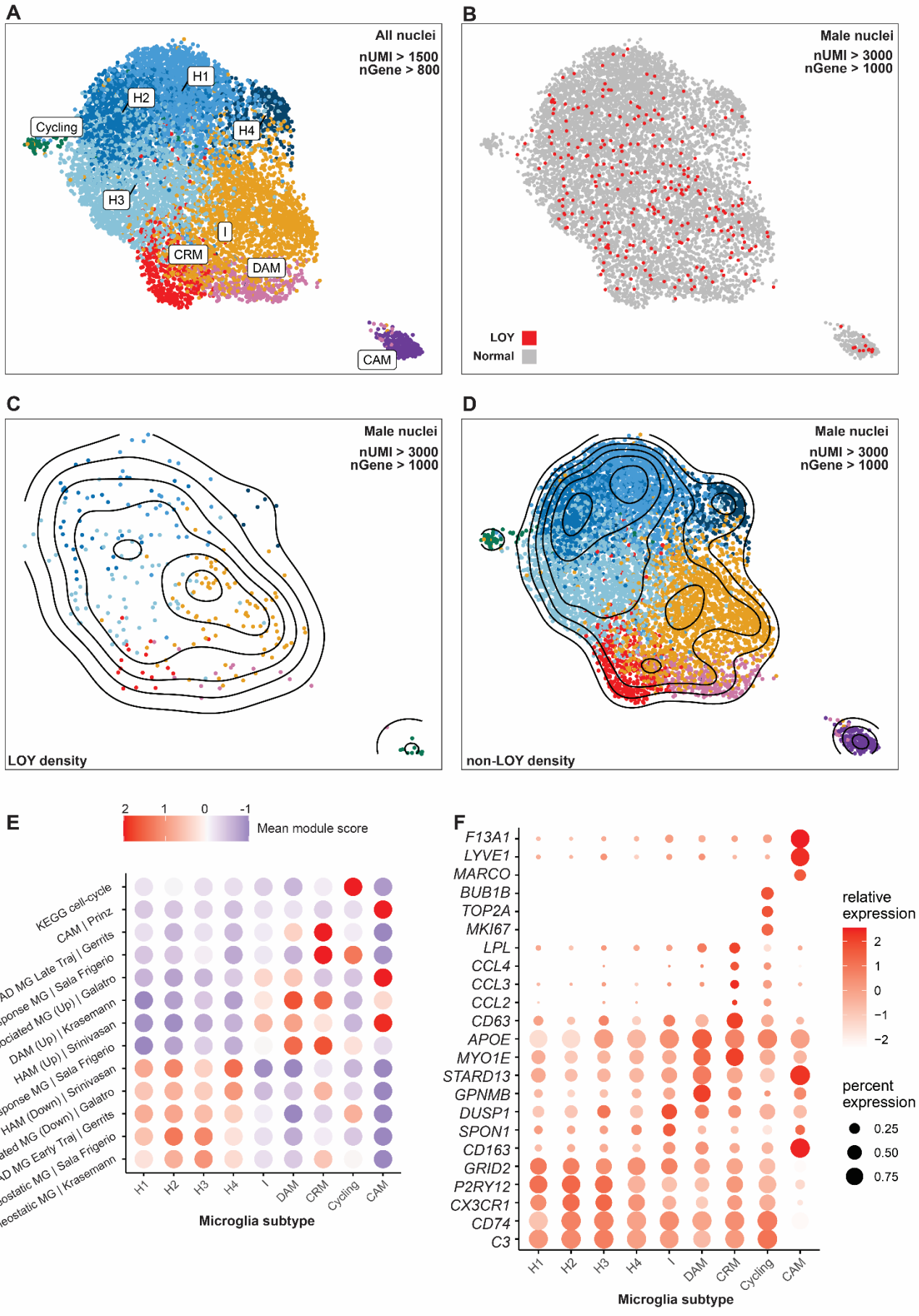
A
All nuclei
nUMI > 1500
nGene > 800
H1
H2
Cycling
H4
H3
I
CRM
DAM
CAM
B
Male nuclei
nUMI > 3000
nGene > 1000
LOY
Normal
C
Male nuclei
nUMI > 3000
nGene > 1000
LOY density
D
Male nuclei
nUMI > 3000
nGene > 1000
non-LOY density
E
2
1
0
-1
Mean module score
KEGG cell-cycle
CAM | Prinz
AD MG Late Traj | Gerrits
Cytokine response MG | Sala Frigerio
Age-associated MG (Up) | Galatro
DAM (Up) | Krasemann
HAM (Up) | Srinivasan
Activated response MG | Sala Frigerio
HAM (Down) | Srinivasan
Age-associated MG (Down) | Galatro
AD MG Early Traj | Gerrits
Homeostatic MG | Sala Frigerio
Homeostatic MG | Krasemann
H1
H2
H3
H4
I
DAM
CRM
Cycling
CAM
Microglia subtype
F
F13A1
LYVE1
MARCO
BUB1B
TOP2A
MKI67
LPL
CCL4
CCL3
CCL2
CD63
APOE
MYO1E
STARD13
GPNMB
DUSP1
SPON1
CD163
GRID2
P2RY12
CX3CR1
CD74
C3
H1
H2
H3
H4
I
DAM
CRM
Cycling
CAM
Microglia subtype
relative expression
2
1
0
−1
−2
percent expression
0.25
0.50
0.75

Supplemental Figure S16C: Microglia subtype characterization and LOY summary (GSE178265).
Microglia from single-nuclei RNAseq data (10x 3' v3) from GEO accession GSE178265 were isolated and reprocessed. (*A*) UMAP plot showing microglia subtype clusters for male (*n* = 8,835) nuclei. Each point represents a nucleus and is coloured by subtype annotation (nUMI > 1500 & nGene > 800). (*B*) UMAP plot illustrating LOY status for each included male microglia (LOY %: 3.7%; *n* = 328). (*C-D*) Density contours for (*C*) LOY nuclei and (*D*) non-LOY nuclei illustrate clustering density patterns for each group. (*E-F*) Heatmaps displaying (*E*) published microglia gene set module scores and (*F*) marker genes/DE genes used to annotate each subcluster. Gene sets used are provided in **Supplemental Table S8**. H1-4 Homeostatic microglia, DAM1 Disease associated microglia, I1 Inflammatory microglia, CRM Cytokine release microglia.

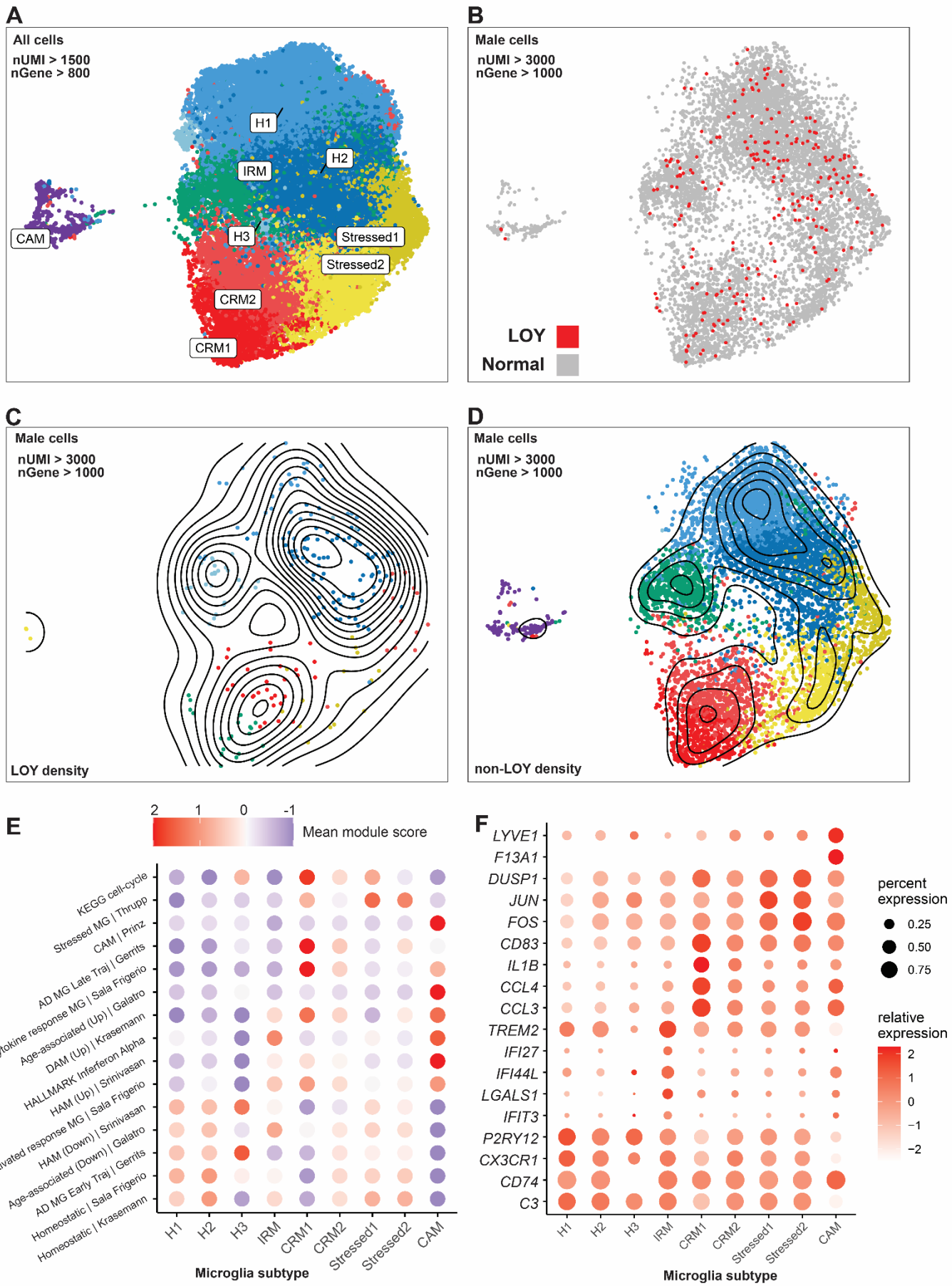
A
All cells
nUMI > 1500
nGene > 800
H1
H2
IRM
H3
CAM
Stressed1
Stressed2
CRM2
CRM1
B
Male cells
nUMI > 3000
nGene > 1000
LOY
Normal
C
Male cells
nUMI > 3000
nGene > 1000
LOY density
D
Male cells
nUMI > 3000
nGene > 1000
non-LOY density
E
2
1
0
-1
Mean module score
KEGG cell-cycle
Stressed MG | Thrupp
CAM | Prinz
AD MG Late Traj | Gerrits
Cytokine response MG | Sala Frigerio
Age-associated (Up) | Galatro
DAM (Up) | Krasemann
HALLMARK Inferferon Alpha
HAM (Up) | Srinivasan
Activated response MG | Sala Frigerio
HAM (Down) | Srinivasan
Age-associated (Down) | Galatro
AD MG Early Traj | Gerrits
Homeostatic | Sala Frigerio
Homeostatic | Krasemann
H1
H2
H3
IRM
CRM1
CRM2
Stressed1
Stressed2
CAM
Microglia subtype
F
LYVE1
F13A1
DUSP1
JUN
FOS
CD83
IL1B
CCL4
CCL3
TREM2
IFI27
IFI44L
LGALS1
IFIT3
P2RY12
CX3CR1
CD74
C3
H1
H2
H3
IRM
CRM1
CRM2
Stressed1
Stressed2
CAM
Microglia subtype
percent expression
0.25
0.50
0.75
relative expression
2
1
0
−1
−2

Supplemental Figure S16D: Microglia subtype characterization and LOY summary (GSE137444). Microglia from single-cell RNAseq data (10x 3' v2) from GEO accession GSE137444 were isolated and reprocessed. (*A*) UMAP plot showing microglia subtype clusters for male (*n* = 11,756) and female nuclei (*n* = 29,284). Each point represents a cell and is coloured by subtype annotation (nUMI > 1500 & nGene > 800). (*B*) UMAP plot illustrating LOY status for each included male microglia (LOY: 233/7039 (3.2%); nUMI > 3000 & nGene > 1000). (*C-D*) Density contours for (*C*) LOY nuclei and (*D*) non-LOY nuclei illustrate clustering density patterns for each group. (*F-E*) Heatmaps displaying (*E*) published microglia gene set module scores and (*F*) marker genes/DE genes used to annotate each subcluster. Gene sets used are provided in **Supplemental Table S8**.
H1-3 Homeostatic microglia, DAM Disease associated microglia, IRM Interferon response microglia, CRM1-2 Cytokine release microglia.

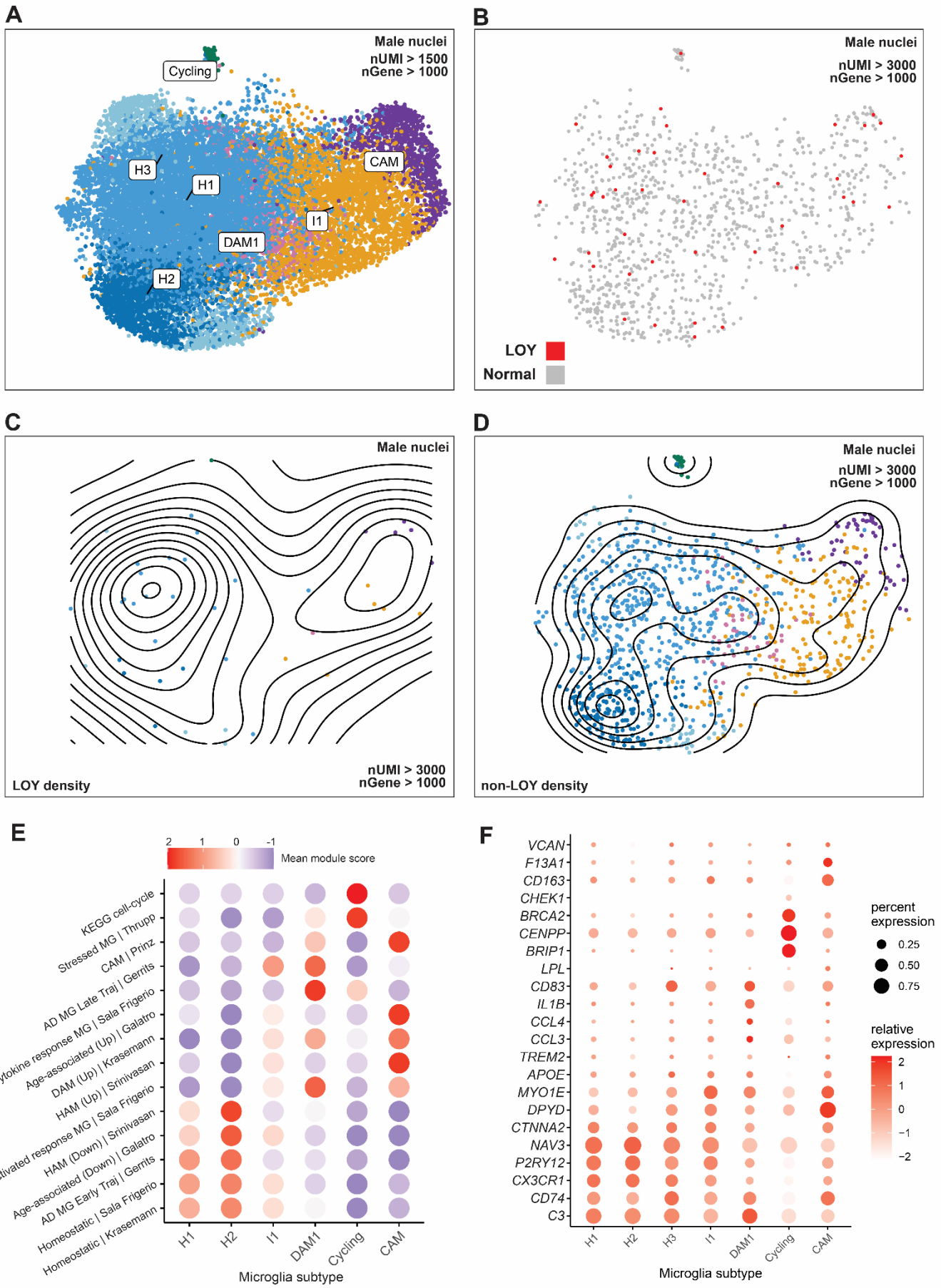
A
Male nuclei
nUMI > 1500
nGene > 1000
Cycling
H3
H1
CAM
I1
DAM1
H2
B
Male nuclei
nUMI > 3000
nGene > 1000
LOY
Normal
C
Male nuclei
LOY density
nUMI > 3000
nGene > 1000
D
Male nuclei
nUMI > 3000
nGene > 1000
non-LOY density
E
2
1
0
-1
Mean module score
KEGG cell-cycle
Stressed MG | Thrupp
CAM | Prinz
AD MG Late Traj | Gerrits
Cytokine response MG | Sala Frigerio
Age-associated (Up) | Galatro
DAM (Up) | Krasemann
HAM (Up) | Srinivasan
Activated response MG | Sala Frigerio
HAM (Down) | Srinivasan
Age-associated (Down) | Galatro
AD MG Early Traj | Gerrits
Homeostatic | Sala Frigerio
Homeostatic | Krasemann
H1
H2
I1
DAM1
Cycling
CAM
Microglia subtype
F
VCAN
F13A1
CD163
CHEK1
BRCA2
CENPP
BRIP1
LPL
CD83
IL1B
CCL4
CCL3
TREM2
APOE
MYO1E
DPYD
CTNNA2
NAV3
P2RY12
CX3CR1
CD74
C3
H1
H2
H3
I1
DAM1
Cycling
CAM
Microglia subtype
percent expression
0.25
0.50
0.75
relative expression
2
1
0
−1
−2

Supplemental Figure S16E: Microglia subtype characterization and LOY summary (GSE148822). Microglia from single-nuclei RNAseq data (10x 3' v3) from GEO accession GSE148822 were isolated and reprocessed. (*A*) UMAP plot showing microglia subtype clusters for 15,737 male nuclei. Each point represents a nucleus and is coloured by subtype annotation (nUMI > 1500 & nGene > 800). (*B*) UMAP plot illustrating LOY status for each included male microglia transcriptome (LOY: 3.7%; nUMI > 3000 & nGene > 1000). (*C-D*) Density contours for (*C*) LOY nuclei and (*D*) non-LOY nuclei illustrate clustering density patterns for each group. (*E-F*) Heatmaps displaying (*E*) published microglia gene set module scores and (*F*) marker genes/DE genes used to annotate each subcluster. Gene sets used are provided in **Supplemental Table S8**.
H1-4 Homeostatic microglia, DAM1-2 Disease associated microglia, I1 Inflammatory microglia, CAM CNS-associated macrophage.

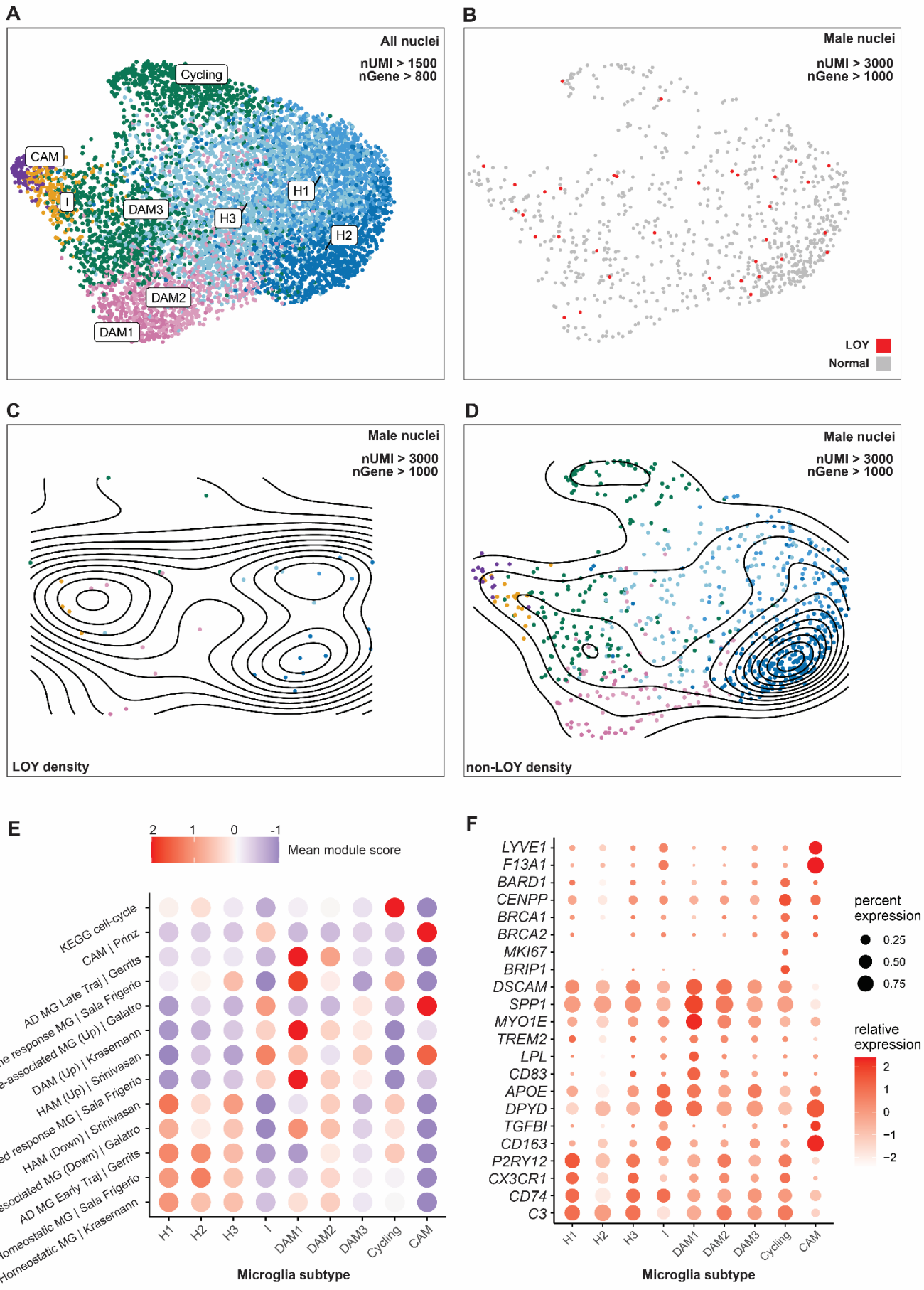
A
All nuclei
nUMI > 1500
nGene > 800
Cycling
CAM
I
DAM3
H3
H1
H2
DAM2
DAM1
B
Male nuclei
nUMI > 3000
nGene > 1000
LOY
Normal
C
Male nuclei
nUMI > 3000
nGene > 1000
LOY density
D
Male nuclei
nUMI > 3000
nGene > 1000
non-LOY density
E
2
1
0
-1
Mean module score
KEGG cell-cycle
CAM | Prinz
AD MG Late Traj | Gerrits
Cytokine response MG | Sala Frigerio
Age-associated MG (Up) | Galatro
DAM (Up) | Krasemann
HAM (Up) | Srinivasan
Activated response MG | Sala Frigerio
HAM (Down) | Srinivasan
Age-associated MG (Down) | Galatro
AD MG Early Traj | Gerrits
Homeostatic MG | Sala Frigerio
Homeostatic MG | Krasemann
H1
H2
H3
I
DAM1
DAM2
DAM3
Cycling
CAM
Microglia subtype
F
LYVE1
F13A1
BARD1
CENPP
BRCA1
BRCA2
MKI67
BRIP1
DSCAM
SPP1
MYO1E
TREM2
LPL
CD83
APOE
DPYD
TGFBI
CD163
P2RY12
CX3CR1
CD74
C3
percent expression
0.25
0.50
0.75
relative expression
2
1
0
−1
−2
H1
H2
H3
I
DAM1
DAM2
DAM3
Cycling
CAM
Microglia subtype

Supplemental Figure S16F: Microglia subtype characterization and LOY summary (GSE174332). Microglia from single-nuclei RNAseq data (10x 3' v3) from GEO accession GSE174332 were reprocessed. (*A*) UMAP plot showing microglia subtype clusters for 10,695 male and 5826 female nuclei. Each point represents a nucleus and is coloured by subtype annotation (nUMI > 1500 & nGene > 800). (*B*) UMAP plot illustrating LOY status for each included male microglia (LOY: 3.9%; nUMI > 3000 & nGene > 1000). (*C-D*) Density contours for (*C*) LOY nuclei and (*D*) non-LOY nuclei illustrate clustering density patterns for each group. (*E-F*) Heatmaps displaying (*E*) published microglia gene set module scores and (*F*) marker genes/DE genes used to annotate each subcluster. Gene sets used are provided in **Supplemental Table S8**.
H1-3 Homeostatic microglia, DAM1-3 Disease associated microglia, I Inflammatory microglia, CAM CNS-associated macrophage.

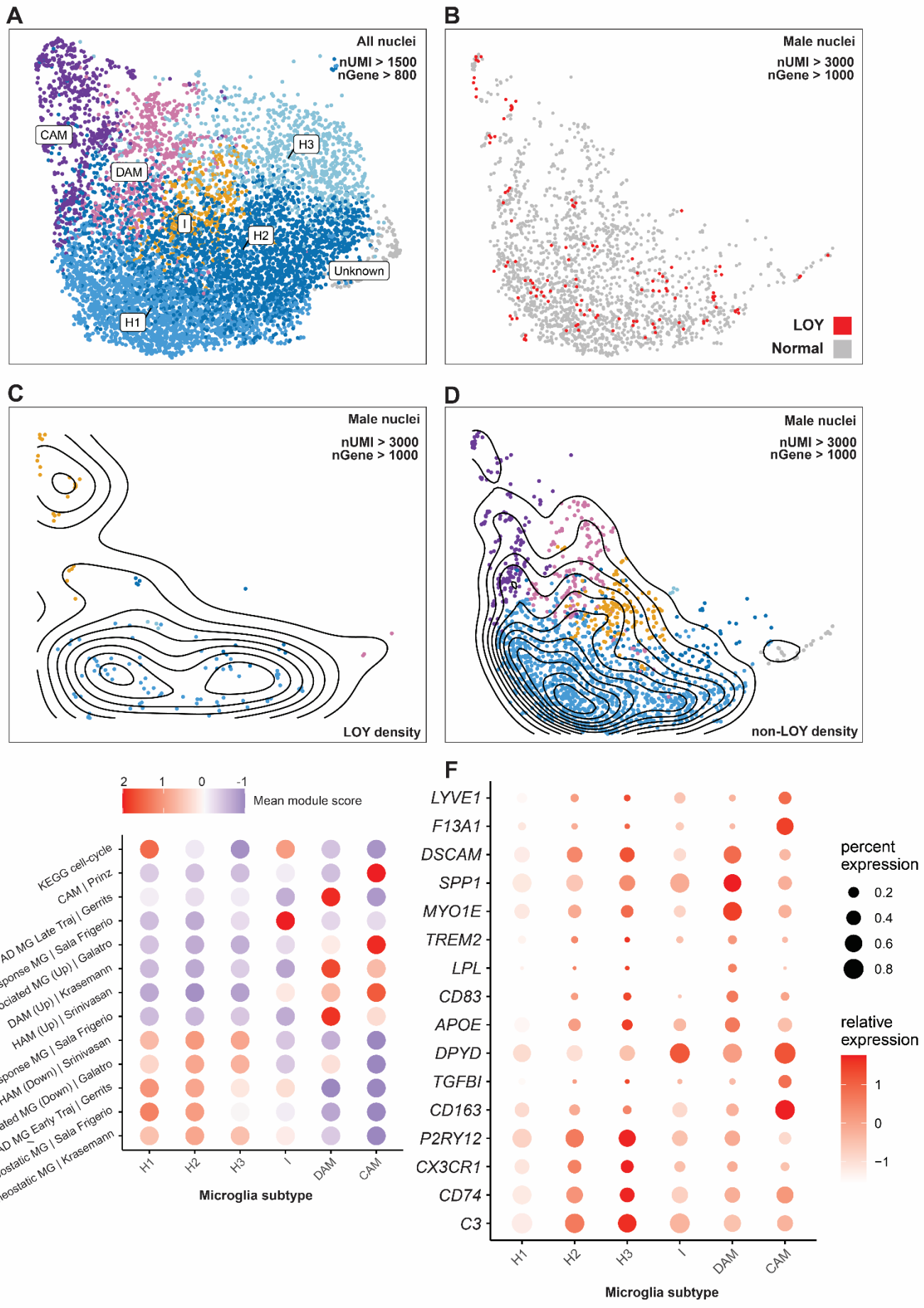
A
All nuclei
nUMI > 1500
nGene > 800
CAM
DAM
H3
I
H2
Unknown
H1
B
Male nuclei
nUMI > 3000
nGene > 1000
LOY
Normal
C
Male nuclei
nUMI > 3000
nGene > 1000
LOY density
D
Male nuclei
nUMI > 3000
nGene > 1000
non-LOY density
E
2
1
0
-1
Mean module score
KEGG cell-cycle
CAM | Prinz
AD MG Late Traj | Gerrits
Cytokine response MG | Sala Frigerio
Age-associated MG (Up) | Galatro
DAM (Up) | Krasemann
HAM (Up) | Srinivasan
Activated response MG | Sala Frigerio
HAM (Down) | Srinivasan
Age-associated MG (Down) | Galatro
AD MG Early Traj | Gerrits
Homeostatic MG | Sala Frigerio
Homeostatic MG | Krasemann
H1
H2
H3
I
DAM
CAM
Microglia subtype
F
LYVE1
F13A1
DSCAM
SPP1
MYO1E
TREM2
LPL
CD83
APOE
DPYD
TGFBI
CD163
P2RY12
CX3CR1
CD74
C3
H1
H2
H3
I
DAM
CAM
Microglia subtype
percent expression
0.2
0.4
0.6
0.8
relative expression
1
0
−1

Supplemental Figure S16G: Microglia subtype characterization and LOY summary (GSE174367). Microglia from single-nuclei RNAseq data (10x 3' v3) from GEO accession GSE174367 were reprocessed. (*A*) UMAP plot showing microglia subtype clusters for 5964 male and 4115 female nuclei. Each point represents a nucleus and is coloured by subtype annotation (nUMI > 1500 & nGene > 1000). (*B*) UMAP plot illustrating LOY status for each included male microglia (LOY: 9.3%, *n* = 557). Density contours for (*C*) LOY nuclei and (*D*) non-LOY nuclei illustrate clustering density patterns for each group. Heatmaps displaying (*E*) published microglia gene set module scores and (*F*) marker genes/DE genes used to annotate each subcluster. Gene sets used are provided in **Supplemental Table S8**. H1-3 Homeostatic microglia, DAM Disease associated microglia, I Inflammatory microglia, CAM CNS-associated macrophage.

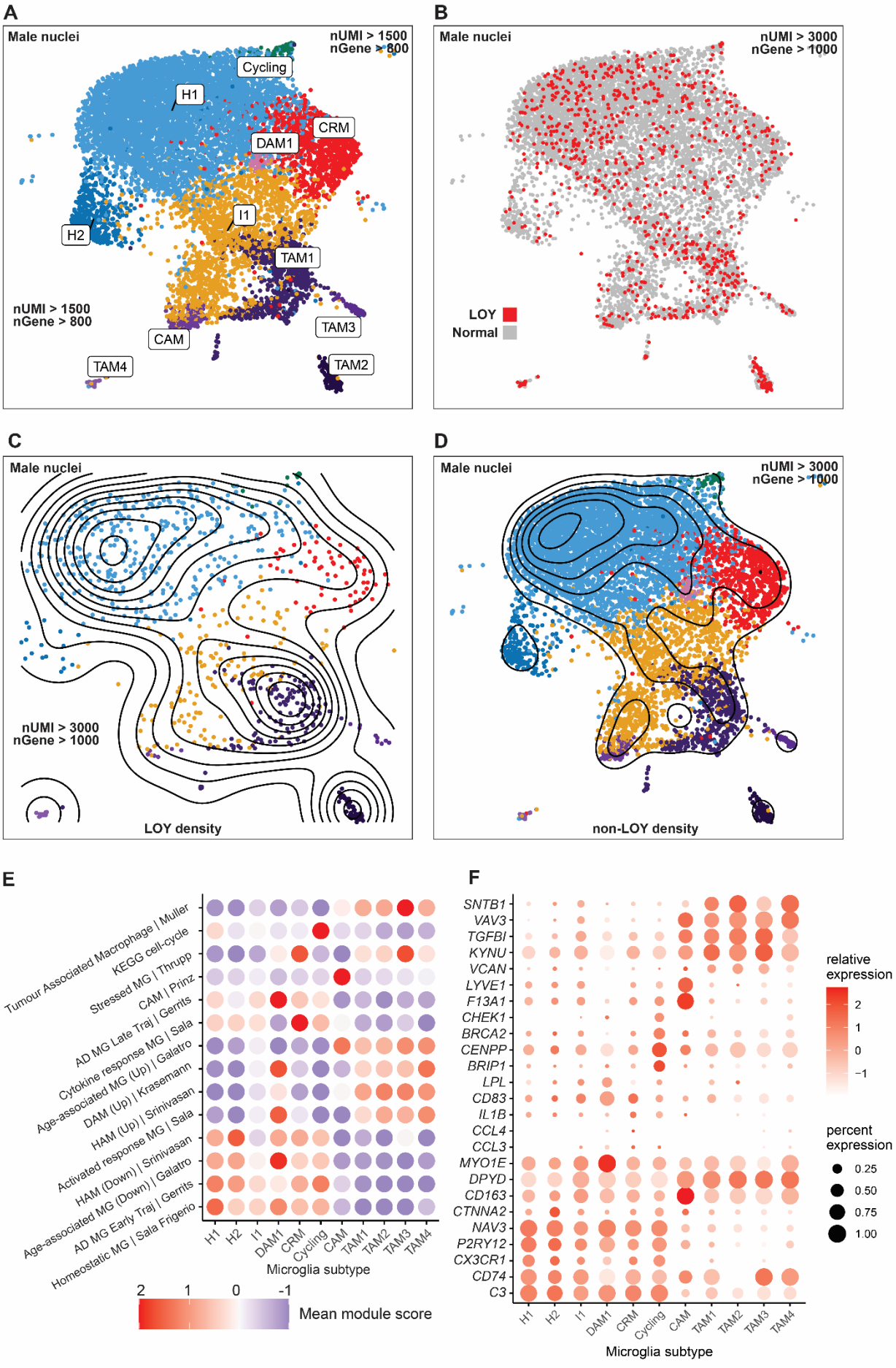
A
Male nuclei
nUMI > 1500
nGene > 800
Cycling
H1
CRM
DAM1
I1
H2
TAM1
TAM3
CAM
TAM4
TAM2
nUMI > 1500
nGene > 800
B
Male nuclei
nUMI > 3000
nGene > 1000
LOY
Normal
C
Male nuclei
nUMI > 3000
nGene > 1000
LOY density
D
Male nuclei
nUMI > 3000
nGene > 1000
non-LOY density
E
Tumour Associated Macrophage | Muller
KEGG cell-cycle
Stressed MG | Thrupp
CAM | Prinz
AD MG Late Traj | Gerrits
Cytokine response MG | Sala
Age-associated MG (Up) | Galatro
DAM (Up) | Krasemann
HAM (Up) | Srinivasan
Activated response MG | Sala
HAM (Down) | Srinivasan
Age-associated MG (Down) | Galatro
AD MG Early Traj | Gerrits
Homeostatic MG | Sala Frigerio
H1 H2 I1 DAM1 CRM Cycling CAM TAM1 TAM2 TAM3 TAM4
Microglia subtype
2 1 0 -1
Mean module score
F
SNTB1
VAV3
TGFBI
KYNU
VCAN
LYVE1
F13A1
CHEK1
BRCA2
CENPP
BRIP1
LPL
CD83
IL1B
CCL4
CCL3
MYO1E
DPYD
CD163
CTNNA2
NAV3
P2RY12
CX3CR1
CD74
C3
H1 H2 I1 DAM1 CRM Cycling CAM TAM1 TAM2 TAM3 TAM4
Microglia subtype
relative expression
2
1
0
−1
percent expression
0.25
0.50
0.75
1.00

Supplemental Figure S16H: Microglia subtype characterization and LOY summary (GSE183068). Microglia from single-nuclei RNAseq data (10x 3' v3) from GEO accession GSE183068 were reprocessed. (*A*) UMAP plot showing microglia subtype clusters for 10,695 male nuclei. Each point represents a nucleus and is coloured by subtype annotation (nUMI > 1500 & nGene > 1000). (*B*) UMAP plot illustrating LOY status for each included male microglia (LOY: 11.8%; nUMI > 3000 & nGene > 1000). Density contours for (*C*) LOY nuclei and (*D*) non-LOY nuclei illustrate clustering density patterns for each group. Heatmaps displaying (*E*) published microglia gene set module scores and (*F*) marker genes/DE genes used to annotate each subcluster. Gene sets used are provided in **Supplemental Table S8**.
H1-2 Homeostatic microglia, DAM1-3 Disease associated microglia, I Inflammatory microglia, CAM CNS-associated macrophage, CRM Cytokine response microglia, TAM Tumor-associated macrophage.

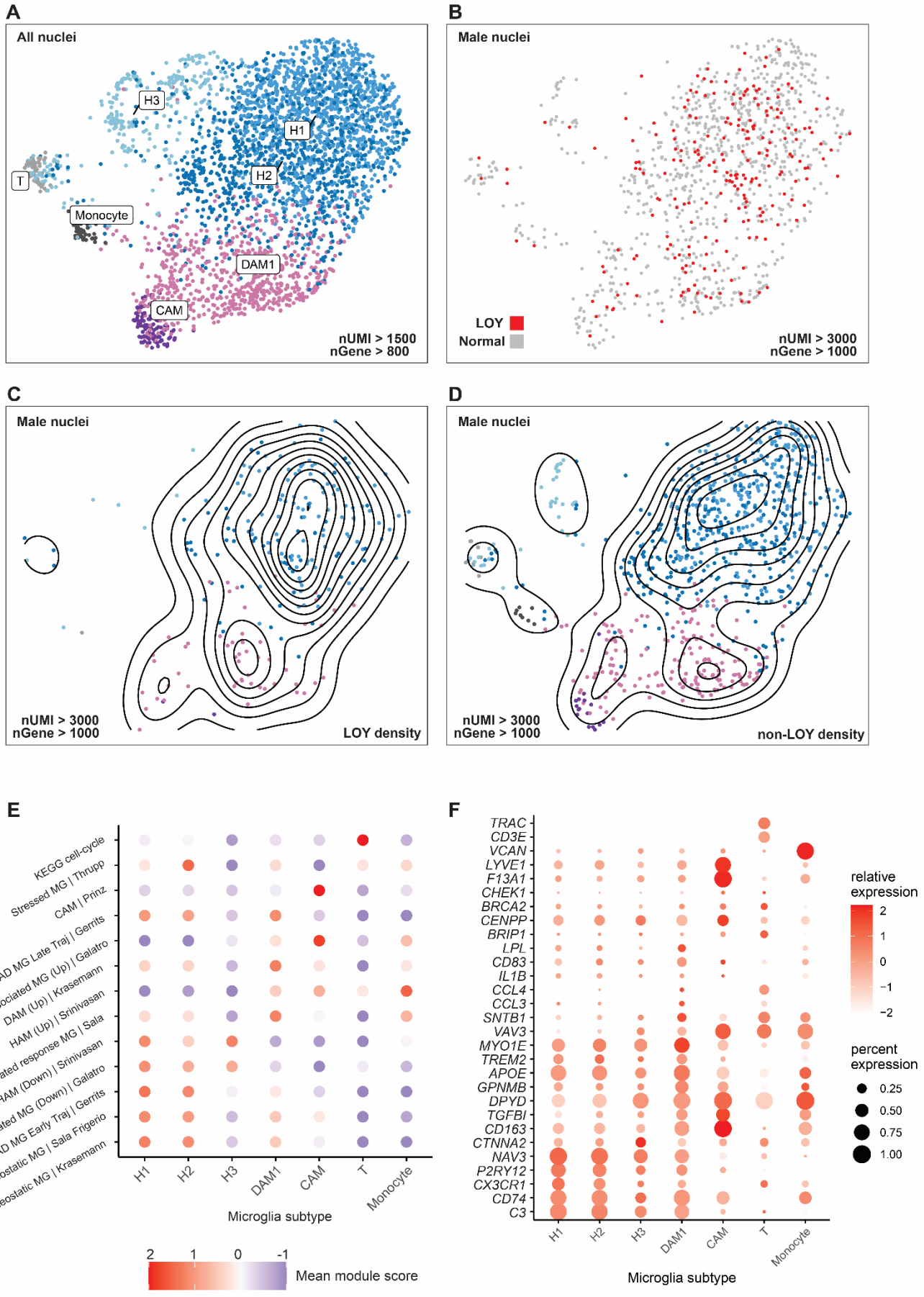
A
All nuclei
H3
H1
H2
T
Monocyte
DAM1
CAM
nUMI > 1500
nGene > 800
B
Male nuclei
LOY
Normal
nUMI > 3000
nGene > 1000
C
Male nuclei
nUMI > 3000
nGene > 1000
LOY density
D
Male nuclei
nUMI > 3000
nGene > 1000
non-LOY density
E
KEGG cell-cycle
Stressed MG | Thrupp
CAM | Prinz
AD MG Late Traj | Gerrits
Age-associated MG (Up) | Galatro
DAM (Up) | Krasemann
HAM (Up) | Srinivasan
Activated response MG | Sala
HAM (Down) | Srinivasan
Age-associated MG (Down) | Galatro
AD MG Early Traj | Gerrits
Homeostatic MG | Sala Frigerio
Homeostatic MG | Krasemann
H1
H2
H3
DAM1
CAM
T
Monocyte
Microglia subtype
2
1
0
-1
Mean module score
F
TRAC
CD3E
VCAN
LYVE1
F13A1
CHEK1
BRCA2
CENPP
BRIP1
LPL
CD83
IL1B
CCL4
CCL3
SNTB1
VAV3
MYO1E
TREM2
APOE
GPNMB
DPYD
TGFBI
CD163
CTNNA2
NAV3
P2RY12
CX3CR1
CD74
C3
H1
H2
H3
DAM1
CAM
T
Monocyte
Microglia subtype
relative expression
2
1
0
−1
−2
percent expression
0.25
0.50
0.75
1.00

Supplemental Figure S16I: Microglia subtype characterization and LOY summary (GSE167494). Microglia from single-nuclei RNAseq data (10x 3' v3) from GEO accession GSE167494 (GSE167490 and GSE167492) were combined and reprocessed. (*A*) UMAP plot showing microglia subtype clusters for 1982 female and 1590 male nuclei. Each point represents a nucleus and is coloured by subtype annotation (nUMI > 1500 & nGene > 1000). (*B*) UMAP plot illustrating LOY status for each included male microglia (LOY: 20.9%). Density contours for (*C*) LOY nuclei and (*D*) non-LOY nuclei illustrate clustering density patterns for each group. Heatmaps displaying (*E*) published microglia gene set module scores and (*F*) marker genes/DE genes used to annotate each subcluster. Gene sets used are provided in **Supplemental Table S8**. H1-3 Homeostatic microglia, DAM1 Disease associated microglia, CAM CNS-associated macrophage.

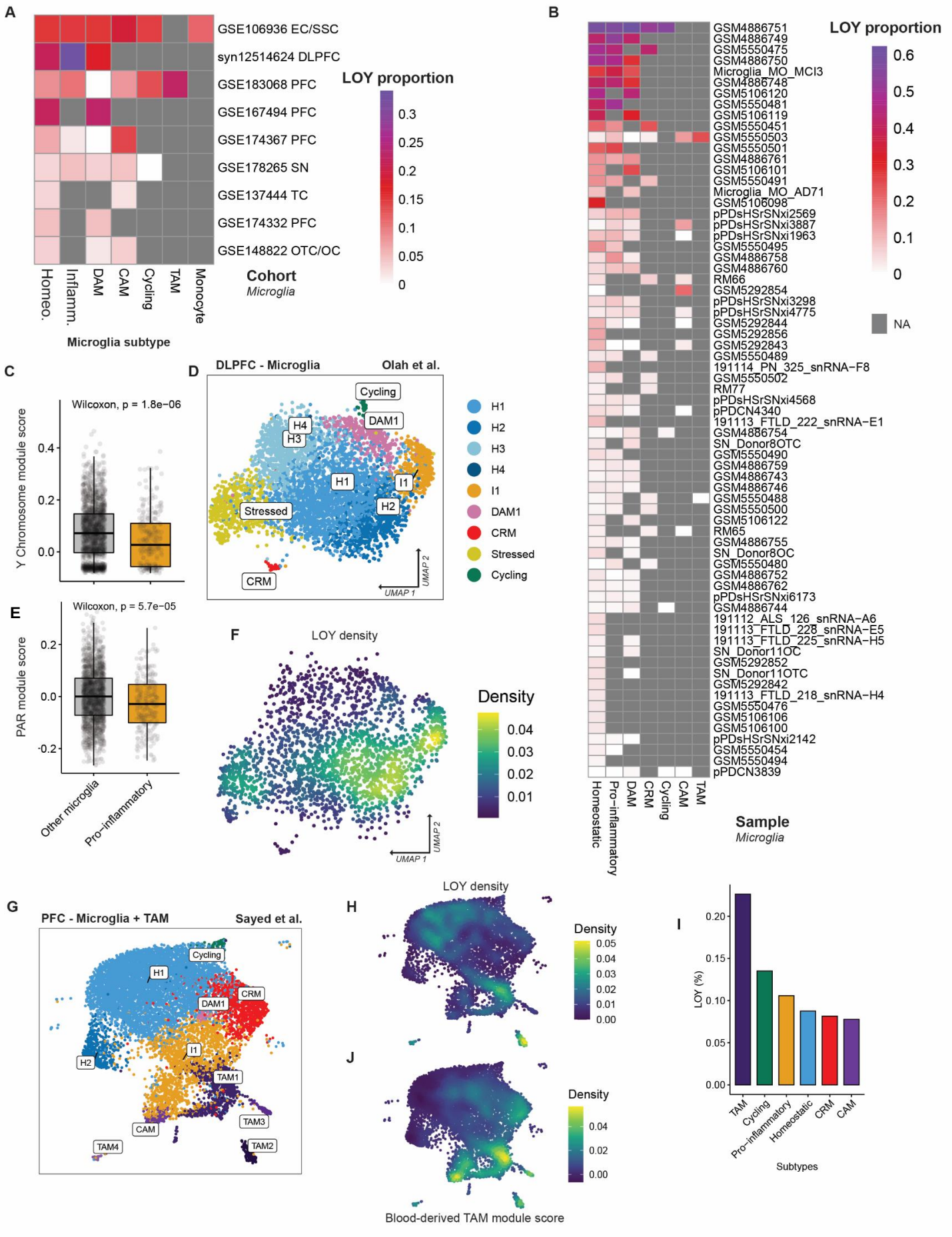
A
GSE106936 EC/SSC
syn12514624 DLPFC
GSE183068 PFC
GSE167494 PFC
GSE174367 PFC
GSE178265 SN
GSE137444 TC
GSE174332 PFC
GSE148822 OTC/OC
Homeo.
Inflamm.
DAM
CAM
Cycling
TAM
Monocyte
Microglia subtype
LOY proportion
0.3
0.25
0.2
0.15
0.1
0.05
0
Cohort
Microglia
B
LOY proportion
0.6
0.5
0.4
0.3
0.2
0.1
0
NA
GSM4886751
GSM4886749
GSM5550475
GSM4886750
Microglia_MO_MCI3
GSM4886748
GSM5106120
GSM5550481
GSM5106119
GSM5550451
GSM5550503
GSM5550501
GSM4886761
GSM5106101
GSM5550491
Microglia_MO_AD71
GSM5106098
pPDsHSrSNxi2569
pPDsHSrSNxi3887
pPDsHSrSNxi1963
GSM5550495
GSM4886758
GSM4886760
RM66
GSM5292854
pPDsHSrSNxi3298
pPDsHSrSNxi4775
GSM5292844
GSM5292856
GSM5292843
GSM5550489
191114_PN_325_snRNA-F8
GSM5550502
RM77
pPDsHSrSNxi4568
pPDCN4340
191113_FTLD_222_snRNA-E1
GSM4886754
SN_Donor8OTC
GSM5550490
GSM4886759
GSM4886743
GSM4886746
GSM5550488
GSM5550500
GSM5106122
RM65
GSM4886755
SN_Donor8OC
GSM5550480
GSM4886752
GSM4886762
pPDsHSrSNxi6173
GSM4886744
191112_ALS_126_snRNA-A6
191113_FTLD_228_snRNA-E5
191113_FTLD_225_snRNA-H5
SN_Donor11OC
GSM5292852
SN_Donor11OTC
GSM5292842
191113_FTLD_218_snRNA-H4
GSM5550476
GSM5106106
GSM5106100
pPDsHSrSNxi2142
GSM5550454
GSM5550494
pPDCN3839
Homeostatic
Pro-inflammatory
DAM
CRM
Cycling
CAM
TAM
Sample
Microglia
C
Wilcoxon, p = 1.8e-06
Y Chromosome module score
0.4
0.2
0.0
D
DLPFC - Microglia
Olah et al.
Cycling
DAM1
H4
H3
H1
I1
H2
Stressed
CRM
UMAP 2
UMAP 1
H1
H2
H3
H4
I1
DAM1
CRM
Stressed
Cycling
E
Wilcoxon, p = 5.7e-05
PAR module score
0.2
0.0
-0.2
Other microglia
Pro-inflammatory
F
LOY density
Density
0.04
0.03
0.02
0.01
UMAP 2
UMAP 1
G
PFC - Microglia + TAM
Sayed et al.
Cycling
H1
CRM
DAM1
I1
H2
TAM1
TAM3
CAM
TAM4
TAM2
H
LOY density
Density
0.05
0.04
0.03
0.02
0.01
0.00
J
Density
0.04
0.02
0.00
Blood-derived TAM module score
I
LOY (%)
0.20
0.15
0.10
0.05
0.00
TAM
Cycling
Pro-inflammatory
Homeostatic
CRM
CAM
Subtypes

Supplemental Figure S17: LOY prevalence in microglia subtypes. Heatmaps showing subtype LOY proportions split by (*A*) cohort and (*B*) individual sample (>3000 nUMI & >1000 nGene). Subtypes were included in (*A*) if they contained >= 50 cells and were included in (*B*) if they contained >= 25 cells. Grey squares denote subtypes that failed to pass the sample size threshold. (*C-F*), LOY microglia are enriched in the pro-inflammatory cluster of syn12514624 (Olah et al. 2020). (*C*) Y Chromosome and (*E*) PAR module scores are significantly reduced in the pro-inflammatory cluster (I1). (*F*) LOY density visualized using kernel density estimation (syn12514624). (*G-I*) LOY is enriched within a cluster of blood-derived tumor-associated microglia/macrophages in GSE183068 (Sayed et al. 2021). (*G*) UMAP plot displaying clustering patterns microglia/macrophages. Density of (*H*) LOY cells and (*J*) TAMs using density kernel estimation. (*I*) Barplot displaying LOY proportions by subtype (GSE183068; >3000 nUMI; >1000 nGene).

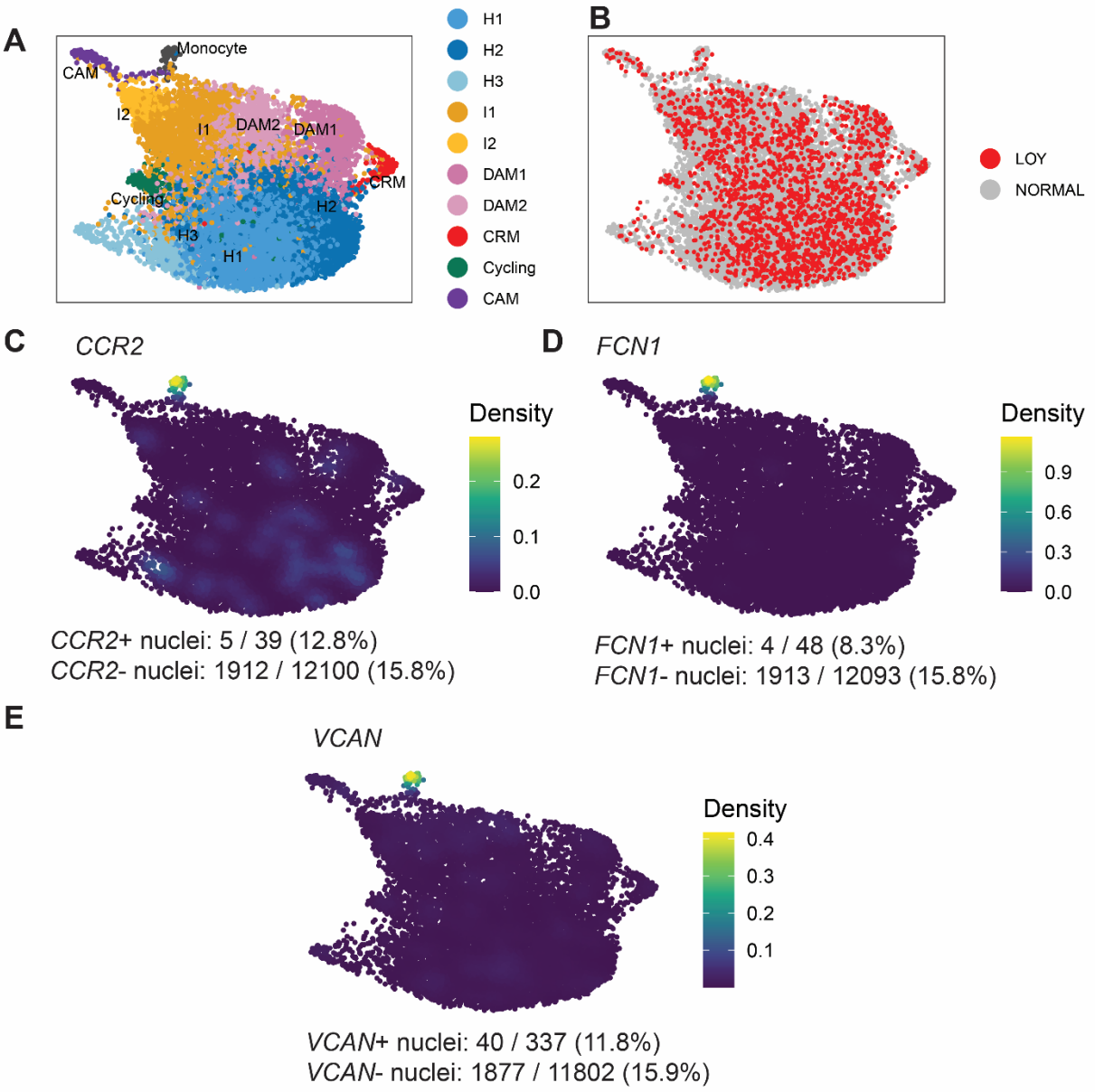

Supplemental Figure S18: Infiltrating monocytes and microglia have similar LOY frequencies (GSE160936)**.** UMAP reductions displaying 12,139 male microglia, monocyte, and CNS associated macrophage (CAM) nuclei from GSE160936 (from the somatosensory cortex and entorhinal cortex). Each point represents an individual nucleus and is colored by (*A*) cluster and (*B*) LOY status. **(***C-E***)** Three microglia UMAP plots displaying kernel gene-weighted density estimation for three known markers of infiltrating monocytes in the CNS (*CCR2*, *VCAN* and *FCN1*) from dataset GSE160936 (Smith et al. 2022). Monocyte expression was confined to one small cluster and was detected in 674 nuclei (2.7%; male and female). Text below each plot displays LOY proportions for male nuclei with and without detected *CCR2*, *VCAN* and *FCN1* expression. Total sample size is provided in parentheses. Nuclei were included if they contained > 3000 nUMI and >1000 nGenes.

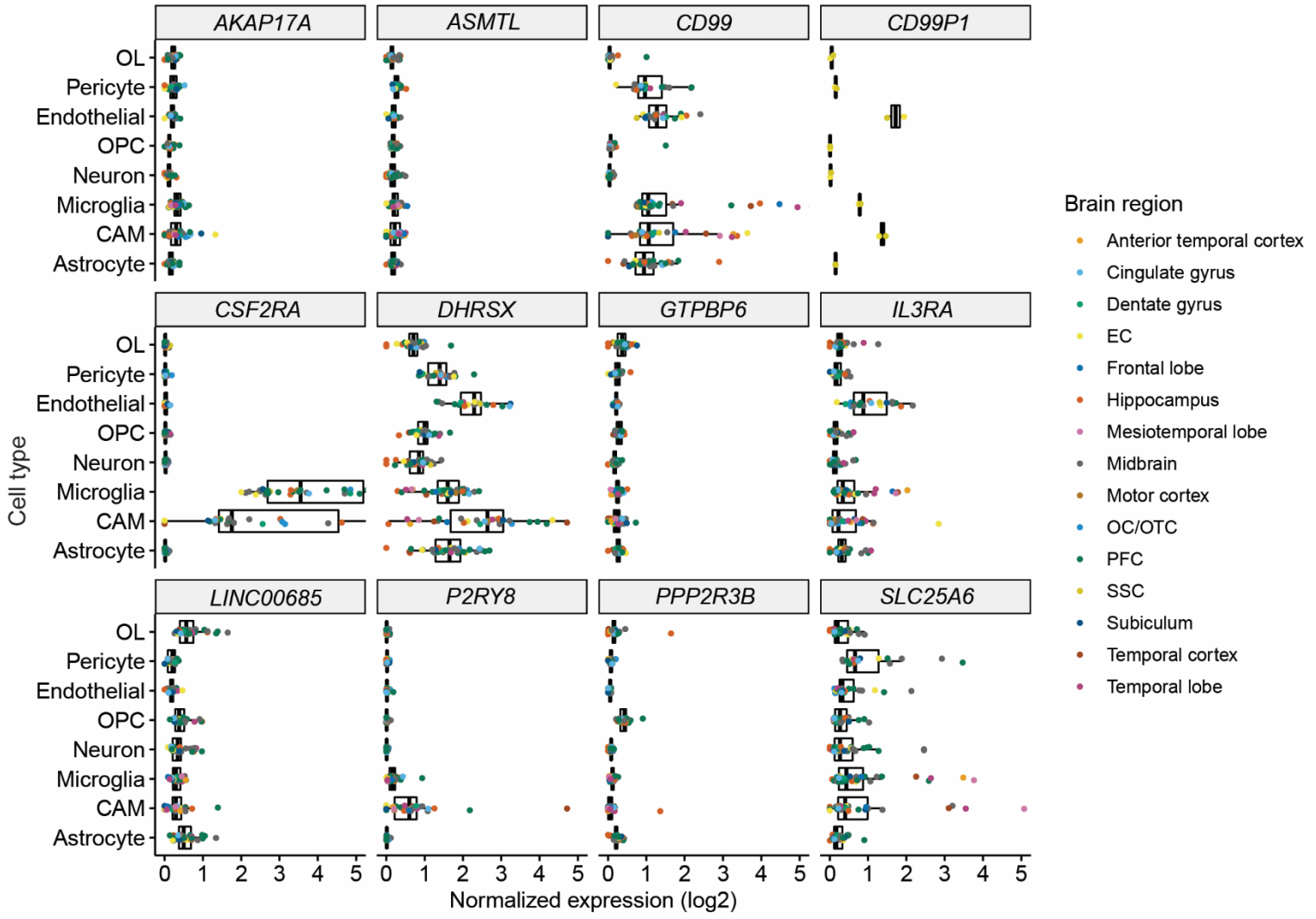

Supplemental Figure S19: PAR gene expression by cell type across 30 brain datasets. Cell type–specific normalized expression (log2) of the top 12 commonly expressed pseudoautosomal region (PAR) genes across 29 brain datasets. Points overlayed on each boxplot are colored by derived brain region and represent a donor/cell type population. OL Oligodendrocyte, CAM CNS-associated macrophage, OPC oligodendrocyte progenitor cell, EC Entorhinal cortex, OC Occipital cortex, OTC Occipitotemporal cortex, PFC Pre-frontal cortex.

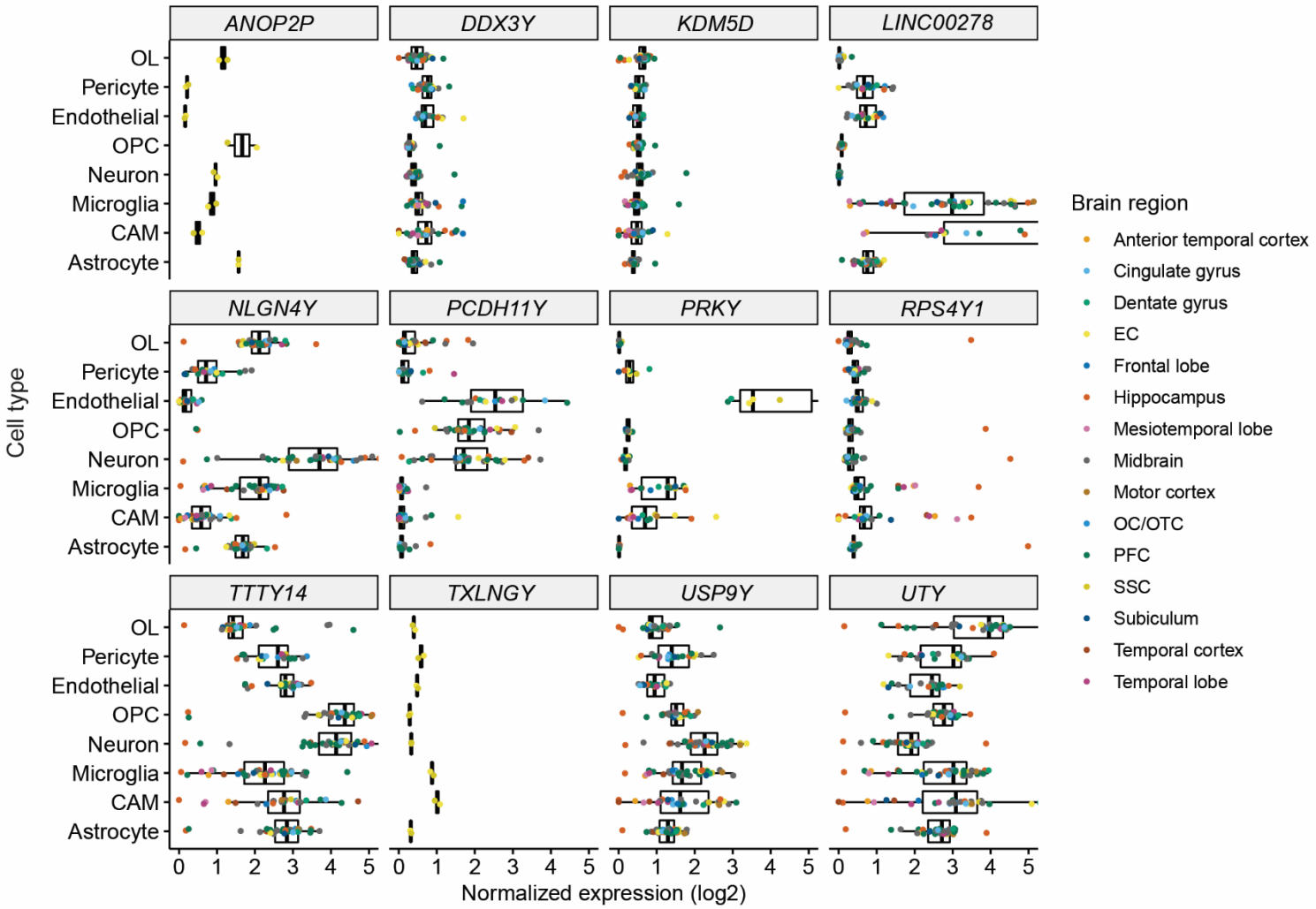

Supplemental Figure S20: Male–specific Y (MSY) gene expression by brain cell type. Cell type–specific normalized expression (log2) of the top 12 most expressed male–specific Y (MSY) genes across 30 brain datasets. Points overlayed on each boxplot are colored by brain region and represent a donor/cell type population. OL Oligodendrocyte, CAM CNS-associated macrophage, OPC oligodendrocyte progenitor cell, EC Entorhinal cortex, OC Occipital cortex, OTC Occipitotemporal cortex, PFC Pre-frontal cortex.

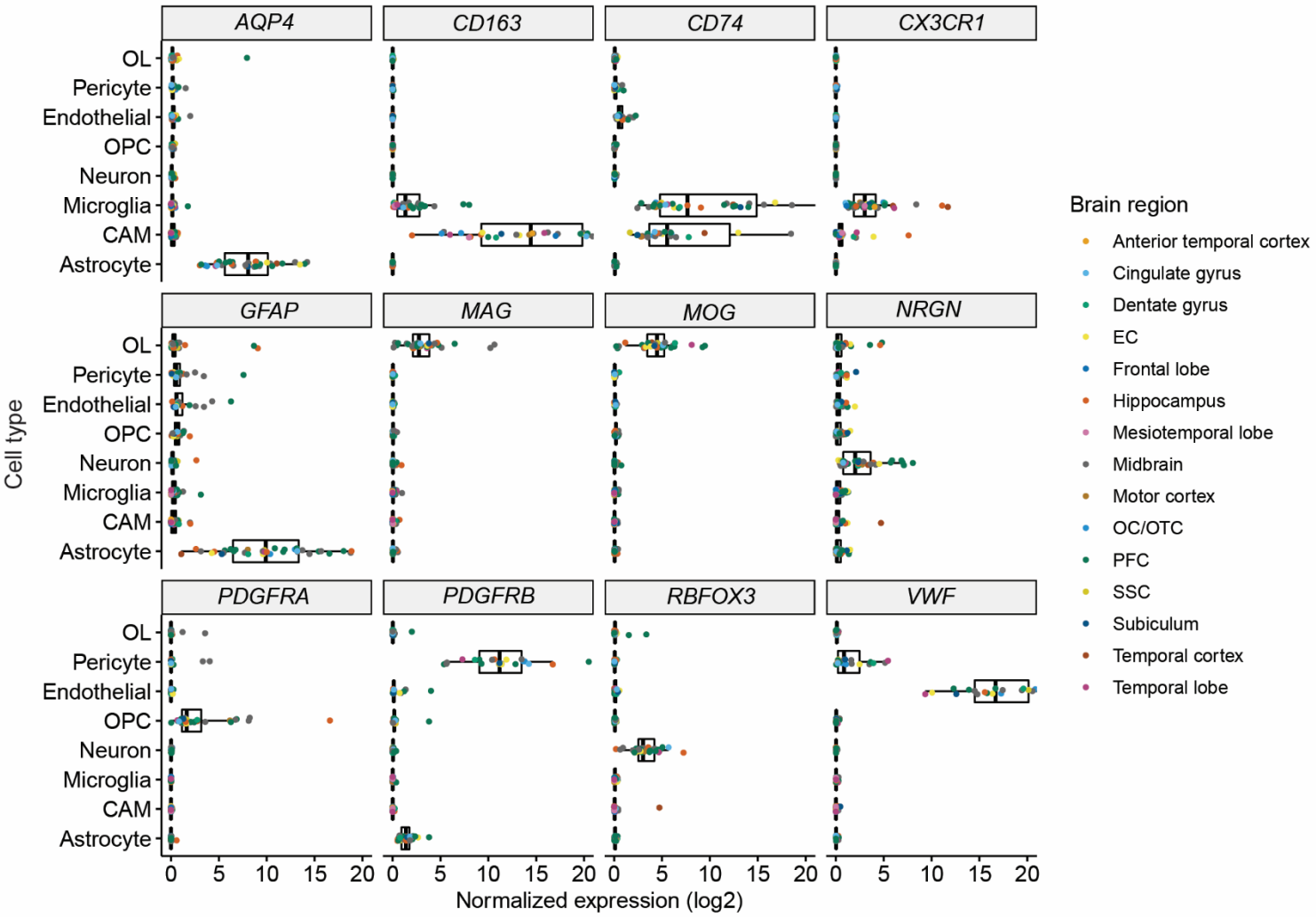

Supplemental Figure S21: Canonical gene markers used to label cell type clusters. Points overlayed on each boxplot are colored by brain region and represent a donor/cell type population. OL Oligodendrocyte, CAM CNS-associated macrophage, OPC oligodendrocyte progenitor cell, EC Entorhinal cortex, OC Occipital cortex, OTC Occipitotemporal cortex, PFC Pre-frontal cortex.

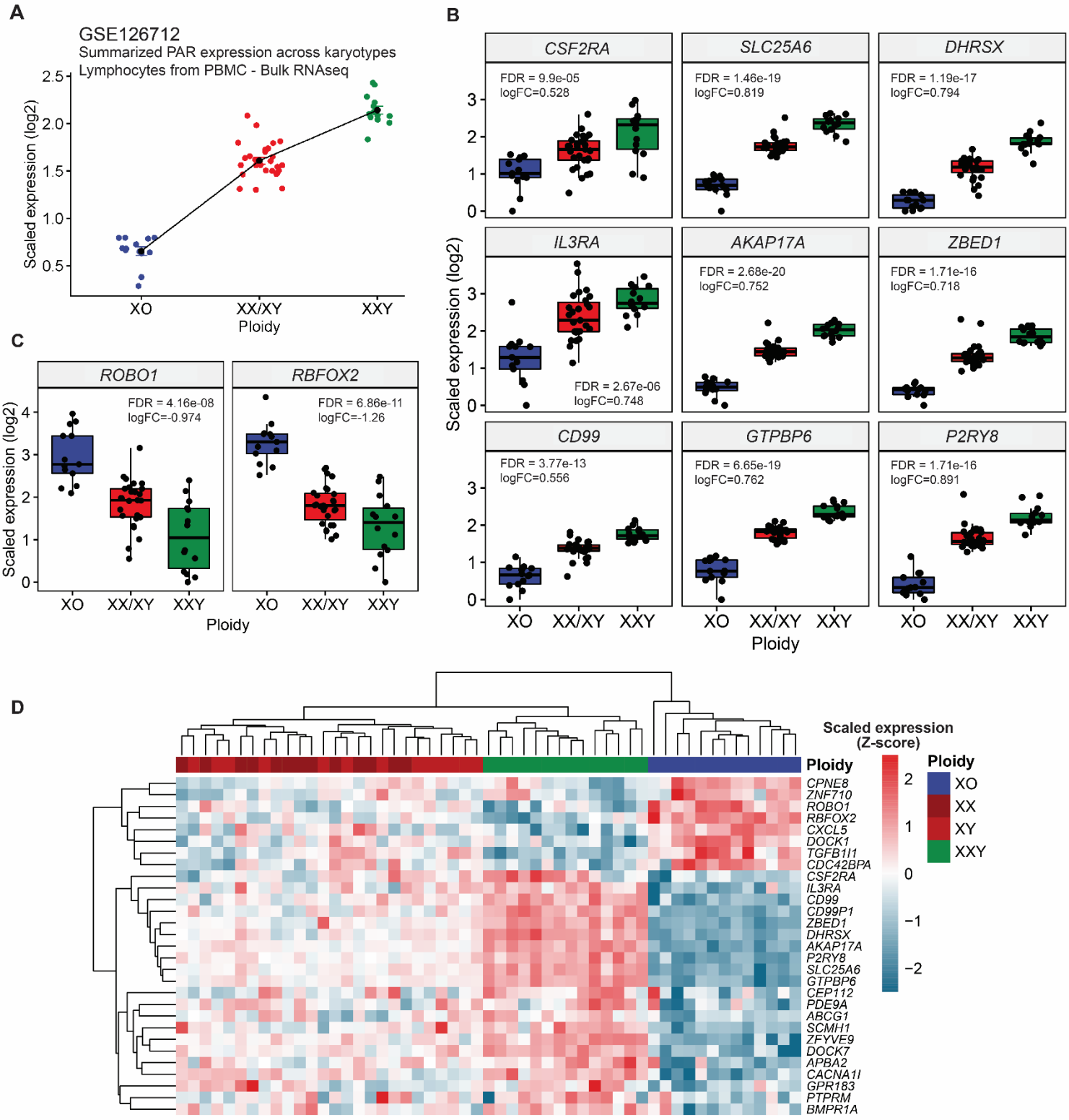

Supplemental Figure S22: PBMC differential expression analysis between XO, XY/XX and XXY donors. Reprocessed data from GEO accession GSE126712. Differential expression analysis using limma voom found 610 DE genes (247 upregulated and 363 downregulated) were associated with increasing sex chromosome ploidy (FDR < 0.01 and absolute value logFC > 0.3). XO, XX/XY and XXY donors have 1, 2 and 3 sex chromosome copies, respectively. (*A*) Line plot illustrating summarized PAR gene expression as sex chromosome ploidy increases. Errors bars represent standard error. (*B-C*) Boxplots displaying normalized expression by karyotype for (*B*) nine expressed PAR genes and (*C*) two recurrently upregulated microglia loss of Y associated transcriptional effect (mLATE) genes in microglia (*ROBO1* and *RBFOX2*). (*D*)

Heatmap illustrating mLATE gene expression in sex chromosome disorder PBMCs. Autosomal feature overlap between LOY microglia DE and sex chromosome ploidy DEs in PBMCs was significant (Fisher's exact test, $P < 0.001$). Columns are colored by sex chromosome karyotype.

Supplemental Tables

Supplementary Table S1 – Included brain scRNA-seq dataset summary
Supplementary Table S2 – Brain cell type LOY summary by donor
Supplementary Table S3 - Summary of 193 LATE genes in microglia and comparison with previously published data.
Supplementary Table S4 - Genomic region enrichment of microglia LATEs by donor
Supplementary Table S5 – microglia LATE gene set enrichment results (Metascape)
Supplementary Table S6 - Summary of subtype–specific microglia LOY estimates by cohort
Supplementary Table S7 - Summary of LOY estimates by monocyte marker status
Supplementary Table S8 – Microglia gene sets used in this study

Supplemental Code

Functions.R – contains all helper R functions for LOY analysis.
call_LOY.R – contains R functions used to call LOY in Seurat objects.
LOY_adjust.R – contains R function to adjust LOY using MSY sparsity.

All functions and scripts used to process data and produce figures can be found at:
https://github.com/michaelcvermeulen/microglia-loss-of-y

Supplemental Data

Supplementary Data S1 – Donor–specific LOY summary files for each cell type across a diverse set of human tissues with increasing UMI depth thresholding. Used for model fitting and MSY sparsity LOY adjustment. All included sc/snRNA-seq datasets in this file are droplet-based 10x Genomics prepared datasets.

Supplementary Data S2 – Donor–specific LOY summary files in brain cell types using 1500 and 3000 UMI depth thresholds. Used for Figure 3 and Figure 4.

References

Aran D, Looney AP, Liu L, Wu E, Fong V, Hsu A, Chak S, Naikawadi RP, Wolters PJ, Abate AR, et al. 2019. Reference-based analysis of lung single-cell sequencing reveals a transitional profibrotic macrophage. *Nat Immunol* **20**: 163–172.

Bunis DG, Andrews J, Fragiadakis GK, Burt TD, Sirota M. 2020. dittoSeq: universal user-friendly single-cell and bulk RNA sequencing visualization toolkit. *Bioinformatics* **36**: 5535–5536.

Dumanski JP, Halvardson J, Davies H, Rychlicka-Buniowska E, Mattisson J, Moghadam BT, Nagy N, Węglarczyk K, Bukowska-Strakova K, Danielsson M, et al. 2021. Immune cells lacking Y chromosome show dysregulation of autosomal gene expression. *Cell Mol Life Sci*. https://doi.org/10.1007/s00018-021-03822-w (Accessed April 28, 2021).

Finak G, McDavid A, Yajima M, Deng J, Gersuk V, Shalek AK, Slichter CK, Miller HW, McElrath MJ, Prlic M, et al. 2015. MAST: a flexible statistical framework for assessing transcriptional changes and characterizing heterogeneity in single-cell RNA sequencing data. *Genome Biol* **16**: 278.

Korsunsky I, Millard N, Fan J, Slowikowski K, Zhang F, Wei K, Baglaenko Y, Brenner M, Loh P, Raychaudhuri S. 2019. Fast, sensitive and accurate integration of single-cell data with Harmony. *Nat Methods* **16**: 1289–1296.

Mattisson J, Danielsson M, Hammond M, Davies H, Gallant CJ, Nordlund J, Raine A, Edén M, Kilander L, Ingelsson M, et al. 2021. Leukocytes with chromosome Y loss have reduced abundance of the cell surface immunoprotein CD99. *Sci Rep* **11**: 15160.

Müller S, Kohanbash G, Liu SJ, Alvarado B, Carrera D, Bhaduri A, Watchmaker PB, Yagnik G, Di Lullo E, Malatesta M, et al. 2017. Single-cell profiling of human gliomas reveals macrophage ontogeny as a basis for regional differences in macrophage activation in the tumor microenvironment. *Genome Biol* **18**: 234.

Olah M, Menon V, Habib N, Taga MF, Ma Y, Yung CJ, Cimpean M, Khairallah A, Coronas-Samano G, Sankowski R, et al. 2020. Single cell RNA sequencing of human microglia uncovers a subset associated with Alzheimer's disease. *Nat Commun* **11**: 6129.

Sayed FA, Kodama L, Fan L, Carling GK, Udeochu JC, Le D, Li Q, Zhou L, Wong MY, Horowitz R, et al. 2021. AD-linked R47H-TREM2 mutation induces disease-enhancing microglial states via AKT hyperactivation. *Sci Transl Med* **13**: eabe3947.

Smith AM, Davey K, Tsartsalis S, Khozoie C, Fancy N, Tang SS, Liaptsi E, Weinert M, McGarry A, Muirhead RCJ, et al. 2022. Diverse human astrocyte and microglial transcriptional responses to Alzheimer's pathology. *Acta Neuropathol (Berl)* **143**: 75–91.

Thrupp N, Sala Frigerio C, Wolfs L, Skene NG, Fattorelli N, Poovathingal S, Fourne Y, Matthews PM, Theys T, Mancuso R, et al. 2020. Single-Nucleus RNA-Seq Is Not Suitable for Detection of Microglial Activation Genes in Humans. *Cell Rep* **32**: 108189.

Zhang X, Hong D, Ma S, Ward T, Ho M, Pattni R, Duren Z, Stankov A, Shrestha SB, Hallmayer J, et al. 2020. Integrated functional genomic analyses of Klinefelter and Turner syndromes reveal global network effects of altered X chromosome dosage. *Proc Natl Acad Sci* **117**: 4864–4873.